









Research Article

Sustained Release of Melatonin from GelMA Liposomes Reduced Osteoblast Apoptosis and Improved Implant Osseointegration in Osteoporosis

Long Xiao ^{1,2}, Jiayi Lin ², Ruoyu Chen ², Yu Huang ^{3,4}, Yu Liu,² Jiaxiang Bai ², Gaoran Ge ², Xiaopeng Shi ¹, Yong Chen ¹, Jiandong Shi ¹, Lu Aiqing ¹, Huilin Yang ², Dechun Geng ² and Zhirong Wang ¹

¹Department of Orthopedics, Zhangjiagang TCM Hospital Affiliated to Nanjing University of Chinese Medicine, Zhangjiagang 215600, China

²Department of Orthopaedics, The First Affiliated Hospital of Soochow University, Suzhou 215006, China

³Department of Gynecology, The First People's Hospital of Zhangjiagang, Soochow University, Zhangjiagang 215600, China

⁴Department of Gynecology, The First Affiliated Hospital of Soochow University, Suzhou 215006, China

Correspondence should be addressed to Dechun Geng; szgengdc@163.com and Zhirong Wang; zjgzzyxl@163.com

Received 10 November 2019; Accepted 25 February 2020; Published 28 May 2020

Academic Editor: Giuseppe Cirillo

Copyright © 2020 Long Xiao et al. This is an open access article distributed under the Creative Commons Attribution License, which permits unrestricted use, distribution, and reproduction in any medium, provided the original work is properly cited.

A reduction in bone mass around an implant is the main cause of implant loosening, especially in postmenopausal osteoporosis patients. In osteoporosis, excessive oxidative stress, resulting in osteoblast apoptosis, largely contributes to abnormal bone remodeling. Melatonin (MT) synthesized by the pineal gland promotes osteoblast differentiation and bone formation and has been effectively used to combat oxidative stress. Therefore, we hypothesized that MT attenuates osteoblast apoptosis induced by oxidative stress, promotes osteogenesis in osteoporosis, and improves bone mass around prostheses. Moreover, considering the distribution and metabolism of MT, its systemic administration would require a large amount of MT, increasing the probability of drug side effects, so the local administration of MT is more effective than its systemic administration. In this study, we constructed a composite adhesive hydrogel system (GelMA-DOPA@MT) to bring about sustained MT release in a local area. Additionally, MT-reduced apoptosis caused by hydrogen peroxide- (H_2O_2 -) induced oxidative stress and restored the osteogenic potential of MC3T3-E1 cells. Furthermore, apoptosis in osteoblasts around the implant was significantly attenuated, and increased bone mass around the implant was observed in ovariectomized (OVX) rats treated with this composite system. In conclusion, our results show that GelMA-DOPA@MT can inhibit osteoblast apoptosis caused by oxidative stress, thereby promoting osteogenesis and improving bone quality around a prosthesis. Therefore, this system of local, sustained MT release is a suitable candidate to address implant loosening in patients with osteoporosis.

1. Introduction

The population in today's society is aging. Among health issues brought about by aging, osteoporosis has become one of the most serious issues and attracted the attention of orthopedist [1–3]. Osteoporosis is a metabolic disease characterized by bone mass loss and bone microstructure destruction, leading to fragility of the bone and increased bone fracture risk [4, 5]. Osteoporosis caused by aging brings about a chain reaction of effects; after implantation, internal fixation screws and

pedicle screws exhibit implantation loosening to different extents, which leads to implantation failure [6–10]. Therefore, improving the stability of internal fixation under the pathological conditions of osteoporosis has become the focus and challenge of orthopedic clinical research.

At present, the use of screws with an enlarged diameter, traditional antiosteoporosis drugs, and bone cement injection are the main treatment methods in clinic [11–13]. Among these methods, systemic antiosteoporosis drugs, such as bisphosphonates, denosumab, raloxifene, and teriparatide,

are used to strengthen the strength of osteoporotic bone internal fixation [14, 15]. As shown through clinical observation, this method can increase bone density in the whole body, but because long-term drug treatment is required and the drug needs to reach the site of action through systemic circulation, the local osteoporotic state of the implant is not significantly improved [16, 17]. In addition, by increasing the diameter and length of internal fixation screws, internal fixation in the osteoporotic vertebral body can be strengthened, increasing its efficacy [18, 19]. In severe osteoporosis patients, pedicle burst fracture occurs easily when the diameter of the screw exceeds 70% of the cross-sectional area of the pedicle, so this method cannot meet the clinical needs of these patients.

Melatonin (MT) is an important steroid hormone secreted by the pineal gland with extensive clinical applications [20]. Specifically, MT is currently widely utilized to regulate various functions, such as the biological rhythm and immune system, and exerts antiaging, antioxidation, and anti-tumor effects [21–24]. Increasing evidence indicates that the production of oxidants and the cellular response to oxidative stress are intricately connected to the fate of implanted biomaterials. It has been demonstrated that osteoporosis-mediated accumulation of reactive oxygen species (ROS) may deleteriously affect the bone regeneration, leading to compromised implant osteointegration [25]. Moreover, recent studies on the influence of MT on hard tissues, such as bone and teeth, have attracted much attention [26, 27]. According to these studies, MT plays an important role in regulating bone formation and bone growth, shows potential in promoting bone differentiation, and is also able to reduce apoptosis caused by oxidative stress, which exerts antiosteoporosis effects [26, 28–30]. Moreover, considering the distribution and metabolism of MT, its systemic administration requires a large amount of the drug, increasing the probability of drug side effects, so the local administration of MT is more effective than its systemic administration. In addition, there have been few *in vivo* experiments on the use of MT locally at implants. Thus, for MT to exert antiosteoporosis effects at local implantation areas, it must be continuously and steadily released over the long term and *in situ*.

Owing to its excellent adhesive ability and biocompatibility, gelatin methacryloyl-dopamine (GelMA-DOPA) has been widely used in bone tissue engineering [31–33]. Liposomes, which are well-known for their excellent biocompatibility and satisfactory ability to control drug release, have been widely utilized in various types of drug delivery [34–36]. In this study, we combined MT with GelMA-DOPA, which has potential adhesive functions on wet surfaces, to fabricate a composite implantation system to induce implant osseointegration in an osteoporotic state by reducing osteoblast apoptosis (Scheme 1).

2. Materials and Methods

2.1. Fabrication and Characterization of GelMA-DOPA

2.1.1. Fabrication of GelMA-COOH. GelMA was fabricated as previously reported [37]. Briefly, 4 g of GelMA was dissolved

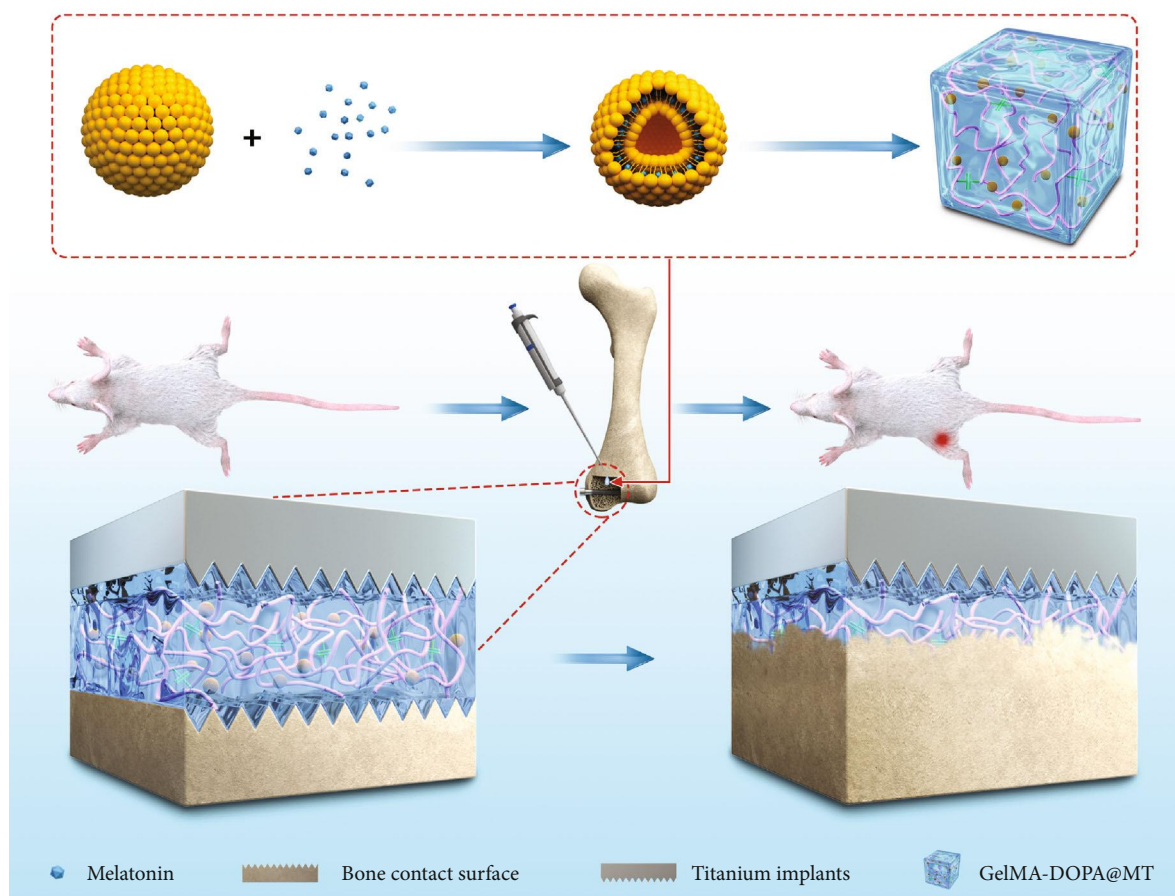
in 80 mL of PBS in a flask by stirring (200 rpm) at 50°C. Then, 2 mL of triethylamine and 2 g of succinic anhydride in 40 mL of DMSO were added to the GelMA mixture. The resulting mixture was stirred overnight at 50°C under the protection of Ar, diluted in 200 mL of PBS, and neutralized with 0.1 M HCl. The product was poured into a dialysis bag (MW = 3500) and dialyzed for approximately one week. The resulting liquid was frozen at -80°C overnight and then lyophilized to obtain GelMA-COOH.

2.1.2. Fabrication of GelMA-DOPA. Catechol motifs are key factors for the successful construction of adhesive materials. To conjugate catechol motifs to GelMA [38], 1 g of GelMA-COOH was dissolved in 10 mL of MES buffer (50 mM, pH 5), and the resulting solution was ultrasonicated for 30 min to remove any air bubbles. Then, 0.2 g of EDC, 0.3 g of NHS, and 0.2 g of dopamine hydrochloride were added to the solution. This whole process was carried out under the protection of Ar, and the mixture was stirred overnight at 25°C. Then, the solution was dialyzed against 0.01 M HCl in deionized water utilizing a dialysis bag (MW = 3500) for 4 days, followed by neutralization with 0.01 M NaOH. The resulting liquid was frozen at -80°C overnight and then lyophilized to obtain GelMA-DOPA.

2.2. Preparation and Characterization of Hydrogel

2.2.1. Preparation of Hydrogel. GelMA, GelMA-COOH, and GelMA-DOPA were dissolved in PBS at concentrations of 20% (*w/v*), and 2-hydroxy-4-(2-hydroxyethoxy)-2-methylpropiophenone was added to the solution at 1% (*w/v*) as a photoinitiator [39]. In addition, GelMA-DOPA was dissolved in PBS at different concentrations ranging from 5% to 20%, and 1% photoinitiator was added to the liquid. The abovementioned precrosslinking solutions were poured separately into a custom-made round mold with a diameter of 15 mm and a depth of 5 mm and then photocrosslinked by ultraviolet (UV) light at 6.9 mW/cm²d (360–480 nm) for 10 sec. Composite hydrogels with different concentrations (5–20%) of GelMA-DOPA and the same amount of MT were constructed using methods similar to those used to prepare the abovementioned hydrogel; the resulting hydrogels were named 5GelMA-DOPA@MT, 10GelMA-DOPA@MT, and 20GelMA-DOPA@MT.

2.2.2. In Vitro Drug Release of Composite Hydrogel. The drug release behavior of different composite hydrogels was explored to determine the MT release curve. All of the drug-loaded composite hydrogels were immersed in PBS at 37°C and shaken at 100 rpm to simulate *in vitro* release. The release medium was replaced by the same volume of fresh PBS at the set time points, and the samples were investigated by high-performance liquid chromatography (HPLC). The analysis was performed with an ODS column (100-5 C18 column, 250 × 4.6 mm, 5.0 μm particle size, J&K Chemical, Ltd., Shanghai) at 30°C. To elute MT, the mobile phase consisted of deionized water and methanol (30:70 *v/v*). The flow rate was 1.0 mL/min, and the detection wavelength was 277 nm.



SCHEME 1: Schematic diagram: the mechanism by which GelMA-DOPA@MT promotes bone regeneration. The continuous melatonin release system is injected around the site where Ti implants are inserted into the bone. This system gradually degrades and releases melatonin, promoting the formation of the new bone around Ti implants.

2.2.3. Water Absorption Experiment. To determine the ability of GelMA-DOPA at different concentrations and different types of hydrogels to absorb water, prepared hydrogel was freeze-dried to obtain lyophilized samples [40]. Subsequently, these samples were weighed (W_0) and immersed in PBS. At each set time point, all of the hydrogels were weighed (W_t); then, a curve to describe the ability of the hydrogel to absorb water was drawn. The percentage of water absorption was calculated by the following formula:

$$\text{Water absorption (\%)} = (W_t - W_0) / W_0 \times 100. \quad (1)$$

2.2.4. In Vitro Degradation Tests. Degradation tests were performed according to previously reported procedures. Briefly, prepared hydrogel was immersed in PBS and incubated at 37°C for 24 h to achieve an equilibrium swelling state. Then, the swollen hydrogel was weighed, and its initial mass was recorded as w_0 . Swollen hydrogel was moved to and incubated in a solution of type II collagenase (2 U/mL) in PBS at 37°C while shaking at 100 rpm. At the set time point, the remaining hydrogel was weighed, and the mass was recorded as w_t and used to describe the extent of degradation.

2.3. Mechanical Characterization

2.3.1. Compression Experiment. Cylindrical crosslinked hydrogel was soaked in PBS at 37°C and incubated for 24 h until the hydrogel was swollen. Different concentrations of GelMA-DOPA ranging from 5 to 20% (w/v) were compressed at a speed of 0.5 mm/min using an equivalence force test instrument. GelMA, GelMA-COOH, GelMA-DOPA, and GelMA-DOPA@MT at 20% were also investigated with a similar method. All slopes in the linear region were utilized to determine the compressive moduli of various hydrogel samples.

2.3.2. Adhesive Characterization of GelMA-DOPA. The adhesive property of GelMA-DOPA was explored by standard lap shear tests with some modifications. Briefly, 200 μL of a precrosslinked solution of GelMA, GelMA-COOH, GelMA-DOPA, or GelMA-DOPA@MT (all of these precrosslinked solutions were at a concentration of 20%) was applied to the surface of the bone. The Ti side of a second bone was put into contact with the precrosslinked liquid, resulting in an overlapping (adhesive-bonded) area of approximately $1.0 \times 2.0 \text{ cm}^2$. After 10 seconds of UV irradiation, the samples were soaked in PBS for 2 h to create wet conditions.

Then, a lap shear test was immediately performed under wet conditions until failure with a 50 N load cell at a speed of 1 mm/min.

2.4. In Vitro Biocompatibility of GelMA-DOPA. To examine the biocompatibility of GelMA-DOPA and its derivative, a cell counting kit-8 (CCK-8) assay was used to quantitatively assess biocompatibility, and a live/dead assay was used to qualitatively assess biocompatibility according to the product's instructions. MC3T3-E1 cells (2000 cells/well) were seeded in a 96-well plate and incubated with the leachates of GelMA, GelMA-DOPA, and GelMA-DOPA@MT. The level of dehydrogenase was measured by CCK-8 assay to indirectly determine the number of live cells at 1-day intervals. Fluorescence microscopy was utilized to observe the images from a live/dead assay at 488 and 568 nm excitation wavelengths. In addition, the cellular adhesion of the hydrogels was investigated by seeding MC3T3-E1 cells (1×10^4 cells/well) on the surface of the abovementioned hydrogels in a 48-well plate. Then, the surfaces of the samples were observed by scanning electron microscopy (SEM) at 1-day intervals.

2.5. Cell Culture. MC3T3-E1 cells were cultured in mineralizing medium (α -minimum essential medium (α -MEM) (HyClone, Logan, UT, USA) containing 10% fetal bovine serum and 1% penicillin-streptomycin) in 5% CO₂ at 37°C. To induce the differentiation of MC3T3-E1 cells, the cells were cultured in osteogenic differentiation medium (Dulbecco's modified Eagle medium containing 10% bovine serum, 100 μ g/mL streptomycin, 100 U/mL penicillin, 50 μ g/mL L-ascorbic acid, 100 nM dexamethasone, and 10 mM β -glycerol phosphate). Hydrogen peroxide (H₂O₂) and MT were purchased from Sigma (St. Louis, MO, USA). 3-TYP (a sirtuin 3 inhibitor) was purchased from Selleck. First, the cells were classified into four experimental groups: the (1) control group, cells treated with α -MEM; the (2) H₂O₂ group, cells treated with α -MEM containing H₂O₂ (400 μ M) once; the (3) MT group, cells treated with α -MEM containing H₂O₂ (400 μ M) and melatonin (10 μ M, dose-simulated melatonin systemic route to local system), and the (4) GelMA-DOPA@MT group, cells treated with α -MEM containing H₂O₂ (400 μ M) once and supplemented with GelMA-DOPA@MT (previously collected 20GelMA-DOPA@MT leachate). The media and melatonin in which the first three groups were grown was changed only every day, and medium containing leachate in which the last group was grown was collected daily. Then, the cells were subsequently classified into five experimental groups: the (1) control group, cells treated with α -MEM for 24 h, the (2) H₂O₂ group, cells treated with α -MEM for 12 h and H₂O₂ (400 μ M) for 12 h, the (3) GelMA-DOPA@MT group, cells pretreated with α -MEM for 12 h and then treated with α -MEM containing H₂O₂ (400 μ M) and GelMA-DOPA@MT (previously collected 20GelMA-DOPA@MT leachate) for 12 h, the (4) 3-TYP group, cells pretreated with 3-TYP (50 μ M) for 12 h and then treated with α -MEM supplemented with H₂O₂ (400 μ M) for 12 h, and the (5) GelMA-DOPA@MT+3-TYP group, cells pretreated with 3-TYP (50 μ M) for 12 h, followed by treatment with α -MEM supplemented with H₂O₂ (400 μ M) and

GelMA-DOPA@MT (previously collected 20GelMA-DOPA@MT leachate) for 12 h.

2.6. Real-Time RT-PCR Analysis. We collected total RNA with TRIzol reagent (Invitrogen). The total RNA concentration was determined by a NanoDrop One (Thermo Fisher, USA), and RNA was used for reverse transcription in a 20 μ L reaction volume including PrimeScript RT Master Mix (Takara, Japan) and PCR amplification in a 20 μ L reaction volume including 10 μ L of Forget-Me-Not qPCR Master Mix (Biotium, USA), 0.5 μ L of each primer, 2 μ L of cDNA, and 7 μ L of RNase-free dH₂O. The reaction was carried out with a LightCycler 96 real-time PCR detection system (Roche, USA). The cycle threshold values were normalized to the level of GAPDH. The following primer sequences were used to amplify ALP, OCN, Osterix, Bax, Bcl-2, Sirt3, and GAPDH: ALP forward 5'-CAGCGGGTAGGAAGCAGTTTC-3' and reverse 5'-CCCTGCACCTCATCCCTGA-3', OCN forward 5'-GAGGCTCTGAGAAGCATAAAA-3' and reverse 5'-AGGGCAATAAGGTAGTGAA-3', Osterix forward 5'-TGAGCTGGAACGTCACGTGC-3' and reverse 5'-AAGA GGAGGCCAGCCAGACA-3', Bax forward 5'-AGACAG GGGCCTTTTTGCTA-3' and reverse 5'-AATTCGCCGGA GACTC-3', Bcl-2 forward 5'-GCTACCGTCGTGACTT CGC-3' and reverse 5'-CCCCACCGAACTCAAAGAAGG-3', Sirt3 forward 5'-GAGCGGCCTCTACAGCAAC-3' and reverse 5'-GGAAGTAGTGAGTGACATTGG-3', and GAPDH forward 5'-GGTGAAGGTCGGTGTGAACG-3' and reverse 5'-CTCGCTCCTGGAAGATGGTG-3'. Each sample was tested three times to reduce mistakes.

2.7. Protein Isolation and Western Blot Analysis. Protein samples were resolved by 15% sodium dodecyl sulfate polyacrylamide gel electrophoresis for 2 h and electrophoretically transmitted to a PVDF membrane (Merck Millipore, USA). After blocking nonspecific binding sites with 5% skim milk for 60 min at room temperature, the membranes were incubated overnight at 4°C with primary antibodies against SIRT3 (1:1000; ab189860), Bax (1:1000; ab32503), Bcl-2 (1:1000; ab59348), ALP (1:1000; ab95462), Osterix (1:500; ab22552), OCN (1:500; ab93876), β -actin (1:1000; ab8227), SOD2 (1:5000; ab13533), and Ac-SOD2 (1:5000; ab137037) (all from Abcam, Cambridge, UK). Then, the membranes were rinsed in Tris-buffered saline with Tween 20 and incubated with the corresponding secondary horseradish peroxidase-conjugated antibodies (1:1000) for 2 h at room temperature. The proteins were detected using chemiluminescent HRP substrates (Millipore Corporation, Billerica, MA, USA).

2.8. ALP Staining. After two weeks of culture in the osteogenic medium, MC3T3-E1 cells were incubated with alkaline phosphatase (ALP) stain. Briefly, we washed MC3T3-E1 cells three times with PBS. After fixation in 4% paraformaldehyde for 15 min, the cells were washed three times with PBS and then incubated in a BCIP/NBT working solution (Beyotime Biotech, Jiangsu, China) in the dark for 20 min. The staining outcomes were observed under a microscope.

2.9. Alizarin Red S Staining. After three weeks of culture in the osteogenic medium, MC3T3-E1 cells were stained with Alizarin red S (ARS). Briefly, we washed MC3T3-E1 cells three times with PBS, followed by fixation in 4% paraformaldehyde for 20 min at 4°C. Then, the cells were rinsed and incubated in an ARS staining solution (pH 4.2; Cyagen Biosciences, Santa Clara, CA, USA) for 20 min. Finally, ddH₂O was used to wash the cells three times.

2.10. TUNEL Staining. After three days of culture in osteogenic medium, MC3T3-E1 cells were examined by a One Step TUNEL Apoptosis Assay Kit (Beyotime Biotech, Jiangsu, China), and the cells were observed under fluorescence microscopy to assess apoptosis.

2.11. Animals. Female Sprague-Dawley (SD) rats (8 weeks old, 250 ± 20 g) were purchased from JOINN Laboratories (Suzhou, China). All of the cells in which the animals were fed were specific pathogen-free- (SPF-) class isolators. Experiments involving animals were approved by the Institute of Animal Care Committee of Zhangjiagang Traditional Chinese Medicine Hospital.

2.12. Surgical Procedures. All of the animals received anesthesia. Bilateral ovariectomy (OVX) was performed in 24 rats, and sham operations were performed in the remaining 6 rats. After 3 months, the bone mineral density (BMD) of all rats was measured using dual-energy X-ray absorptiometry (DEXA; Lunar Corporation, Madison, WI, U.S.) to assess whether the osteoporosis model had been successfully developed. Once success was determined, 30 rats underwent bilateral distal femoral titanium screw implantation with sterilized titanium screws (Adil, Suzhou, China). The implants were placed laterally into the distal femur of each rat. Depending on the group, no specific drugs were injected around the implant. Then, the 30 animals were randomly classified into five groups: implant only (control group), ovariectomy+implant (OVX group), OVX+implant+GelMA (GelMA group), OVX+implant+MT (MT group), and OVX+implant+GelMA-DOPA@MT (GelMA-DOPA@MT group) with each group including 6 animals. The MT and GelMA-DOPA@MT groups received the daily i.p. administration of MT (Sigma) at 50 mg/kg of body weight between 5:00 pm and 6:00 pm for 4 weeks following implant installation, while rats in the other groups were injected with normal saline under the same conditions. In addition, all of the rats were injected i.p. 10 mg/kg calcein (Sigma) 10 and 2 days before euthanasia. In the last part of the experiment, the rats were sacrificed, followed by the collection of their bilateral femurs for subsequent studies.

2.13. Radiological Analyses. Femurs containing the titanium implants ($n = 6$ in each group) were measured with high-resolution microcomputed tomography (μ CT, SkyScan 1176; SkyScan, Knotich, Belgium). The femurs were scanned with 18 μ m per layer, and the X-ray parameters were set at a voltage of 50 kV, a current of 500 μ A, and a 0.7° rotational step. A round region with a diameter of 1.8 mm around one-third along the titanium rods of distal femurs was chosen to evaluate related morphometric parameters, including

BMD (g/cm^3), bone volume/total volume (BV/TV, %), bone surface/bone volume (BS/BV, 1/mm), bone surface/total volume (BS/TV, 1/mm), and trabecular number (TbN, 1/mm). Relevant three-dimensional (3D) images were analyzed after processing.

2.14. Histological and Immunohistochemical Analyses. All of the femurs were preserved at 4°C for histological and immunohistochemical analyses after μ CT. Each entire left femur ($n = 6$ per group) was used for hard tissue section staining. After embedded with epoxy resin (45347, Sigma), each specimen was cut into 10 μ m thick sections along the vertical axis with a hard tissue slicer (EXAKT 300CP, Germany). The obtained hard tissue sections were used for calcein staining, whose images determined by fluorescence microscopy. And the mineral apposition rate (MAR) was calculated using Bioquant Osteo 2017 (BIOQUANT Image Analysis Corporation, USA).

The complete femurs were decalcified for 1 month with 15% ethylenediaminetetraacetic acid (EDTA, Sigma), and the specimens (right rat femurs, $n = 6$ per group) were embedded in paraffin after the Ti screws had been removed. Cutting the specimens into 5 μ m sections which used for hematoxylin and eosin (H&E) staining. Finally, sealed the sections by means of neutral balsam (Solarbio) and photographed. With optical microscopy, the BV/TV and inflammatory area were calculated using Bioquant Osteo 2017.

For immunofluorescence staining and terminal deoxynucleotidyl transferase dUTP nick end labeling (TUNEL) staining (Beyotime Biotech, China). The selected region of interest (ROI) was around the Ti screws below the epiphysis. In brief, the sections were dewaxed with xylene and then subjected to gradient hydration and antigen retrieval with hyaluronidase for 1 h at 37°C and pepsin for 25 min at room temperature. The sections were then blocked with serum for 30 min. Next, the paraffin sections were incubated with primary antibodies ALP (ab95462) and Rux2 (ab192256) (all from Abcam) for 12 h at 4°C. Subsequently, the sections were rinsed with PBS and incubated with secondary antibodies (ab150077) for 60 min at room temperature in dark. Then, the sections were rinsed with PBS and incubated with TUNEL test solution for 30 min at 37°C. Afterwards, rinsed with PBS and added mounting medium with DAPI (ab104139). Finally, the slides were stored in the dark at 2-8°C for 10 min and determined by fluorescence microscopy. Positive staining was determined by Bioquant Osteo 2017. The selected region of interest (ROI) was around the Ti screws below the epiphysis.

2.15. Statistical Analysis. Results are represented as the means ± standard deviations. The Kolmogorov-Smirnov test was employed to test statistical normality. Statistical significance was determined by one-way ANOVA with the Tukey's multiple comparisons test employing SPSS 25.0, with $p < 0.05$ indicating a statistically significant difference.

3. Results

3.1. In Vitro Characterization of GelMA-DOPA@MT. The drug release behaviors of GelMA-DOPA with different

amounts of MT liposomes were investigated *in vitro*. As shown in Figure 1(a), the samples exhibited various release characteristics because of differences in their hydrogel network. Among the samples, 5GelMA-DOPA@MT showed the shortest sustained release period of approximately 5 days, and 20GelMA-DOPA@MT exhibited the longest continuous release time of almost 25 days. Differences in the release characteristics between the samples can be attributed to the density of the hydrogel network. For example, 5GelMA-DOPA@MT had the loosest hydrogel network, while 20GelMA-DOPA@MT exhibited the densest hydrogel construction. 20GelMA-DOPA@MT released an inconspicuous burst of MT in the first few days and continuously released MT for approximately 20 days, which laid the groundwork to promote bone regeneration.

As they are important characteristics, the water absorption and degradation of the hydrogels were explored. As shown in Figure 1(b), when hydrogels were prepared at the same concentration (20%), there was no dramatic difference in water absorption among hydrogels composed of different materials (GelMA, GelMA-COOH, GelMA-DOPA, and GelMA-DOPA@MT). As shown in Figure 1(c), there were significant differences in water absorption among hydrogels at different concentrations (5-20%), and water absorption ranged from $614.2 \pm 54.9\%$ for 5GelMA-DOPA to 382.8 ± 6.2 for 20GelMA-DOPA. However, degradation of the hydrogels exhibited a tendency similar to that of water absorption, as shown in Figures 1(d) and 1(e). Hydrogels at the same concentration (20%) degraded at similar rates, indicating that GelMA, GelMA-COOH, GelMA-DOPA, and GelMA-DOPA@MT would be completely degraded after 27 days of soaking. Meanwhile, hydrogels at various concentrations degraded for different lengths of time ranging from 5 days for 5GelMA-DOPA to 28 days for 20GelMA-DOPA.

In implantation, the ability to bear certain external force is crucial; thus, we further characterized GelMA hydrogels with different modifications by compression testing. As shown in Figures 1(f) and 1(g), there were no notable differences in the compression moduli of hydrogels at the same concentration, which were 36.5 ± 1.9 kPa for GelMA, 37.4 ± 2.1 kPa for GelMA-DOPA, and 37.0 ± 2.5 kPa for GelMA-DOPA@MT. Drug-loaded composite hydrogels exhibited mechanical properties similar to those of the other three groups, providing an excellent foundation for multifunctional implants. Moreover, according to the results shown in Figures 1(h) and 1(i), the compression test indicated the expected positive correlation between GelMA-DOPA concentrations and the compressive moduli of the resulting hydrogels, which ranged from 11.6 ± 1.5 kPa for 5GelMA-DOPA hydrogels to 36.1 ± 1.8 kPa for 20GelMA-DOPA hydrogels.

Considering the working conditions of implants, improving adhesion to the surfaces of bones and Ti in wet environments is critical to the success of a multifunctional hydrogel. Therefore, lap shear tests were performed to characterize the *in vitro* adhesive properties of various kinds of GelMA-DOPA under a wet environment. As shown in Figures 1(j) and 1(k), GelMA and GEL-COOH showed limited adhesive properties, but GelMA-DOPA and GelMA-DOPA@MT

exhibited significant adhesive properties. The lap shear strength, which ranged from 9.6 ± 1.9 kPa for 5GelMA-DOPA hydrogels to 46.7 ± 4.9 kPa for 20GelMA-DOPA hydrogels, increased with increasing GelMA-DOPA concentration. This indicates that increasing prepolymer concentrations with an increased DOPA content improves adhesion.

In order to quantify cell proliferation, CCK-8 assays were carried out at 1-day intervals, as shown in Figure 1(l) and Table S1. The optical density (OD) among the four groups was not significantly different and ranged from 0.3 after 1 day to 2.5 after 7 days. Furthermore, cell viability was observed by live/dead staining after 7 days of incubation. As shown in Figure 2(a), the cells in all groups exhibited high viability and excellent dispersion, which shows that GelMA-DOPA@MT exhibits suitable cytocompatibility. In addition, MC3T3-E1 cells were seeded on the surface of different hydrogels, and their cellular morphology and adherence were monitored. The SEM images shown in Figure 2(b) reveal that cells grown on the surface of GelMA-DOPA@MT had a morphology similar to that of cells grown on the GelMA surface at the same time points, indicating that the presence of MT and drug release did not affect cell adherence.

All of the abovementioned results suggest that the ability of GelMA-DOPA@MT to promote MC3T3-E1 cell adhesion and proliferation was not significantly different from that observed in the GelMA, GelMA-DOPA, and control groups, establishing the foundation for further research.

3.2. GelMa-DOPA@MT Promotes the Differentiation of Osteoblasts and Inhibits Their Apoptosis. As shown in Figure 3(a), after MC3T3-E1 cells in different groups underwent treatment, ALP staining showed that the number of positive cells decreased significantly after H₂O₂ treatment compared with that in the control group. However, drug intervention reversed this phenomenon. Quantitative analysis indicated more positive cells in the GelMA-DOPA@MT group than in the MT group. Similar results were also observed by ARS staining. The number of calcium nodules in the H₂O₂ group was extremely small but significantly increased by drug intervention, especially that in the GelMA-DOPA@MT group. Quantitative analysis also indicated that the GelMA-DOPA@MT group exhibited increased osteogenesis (by 1.2-fold vs. the MT group).

To further observe the ability of GelMA-DOPA@MT to induce osteogenic differentiation, RT-PCR showed that after induction by H₂O₂, the mRNA levels of Osterix (0.7-fold, Figure 3(h)), ALP (0.69-fold, Figure 3(i)), and OCN (0.6-fold, Figure 3(j)) were decreased compared with those in the control group. However, drug intervention reversed this phenomenon. As expected, GelMA-DOPA@MT obviously increased gene expression compared with that in the MT group (ALP, 1.1-fold; OCN, 1.4-fold; and Osterix, 1.2-fold). Western blotting showed increased protein levels of ALP, OCN, and Osterix in the GelMA-DOPA@MT group even in the presence of H₂O₂ (Figures 3(d)–3(g)). In addition, similar results were observed in rat BMSCs, and GelMA-DOPA@MT significantly attenuated H₂O₂-induced inhibition on osteoblastic differentiation (Figure S1).

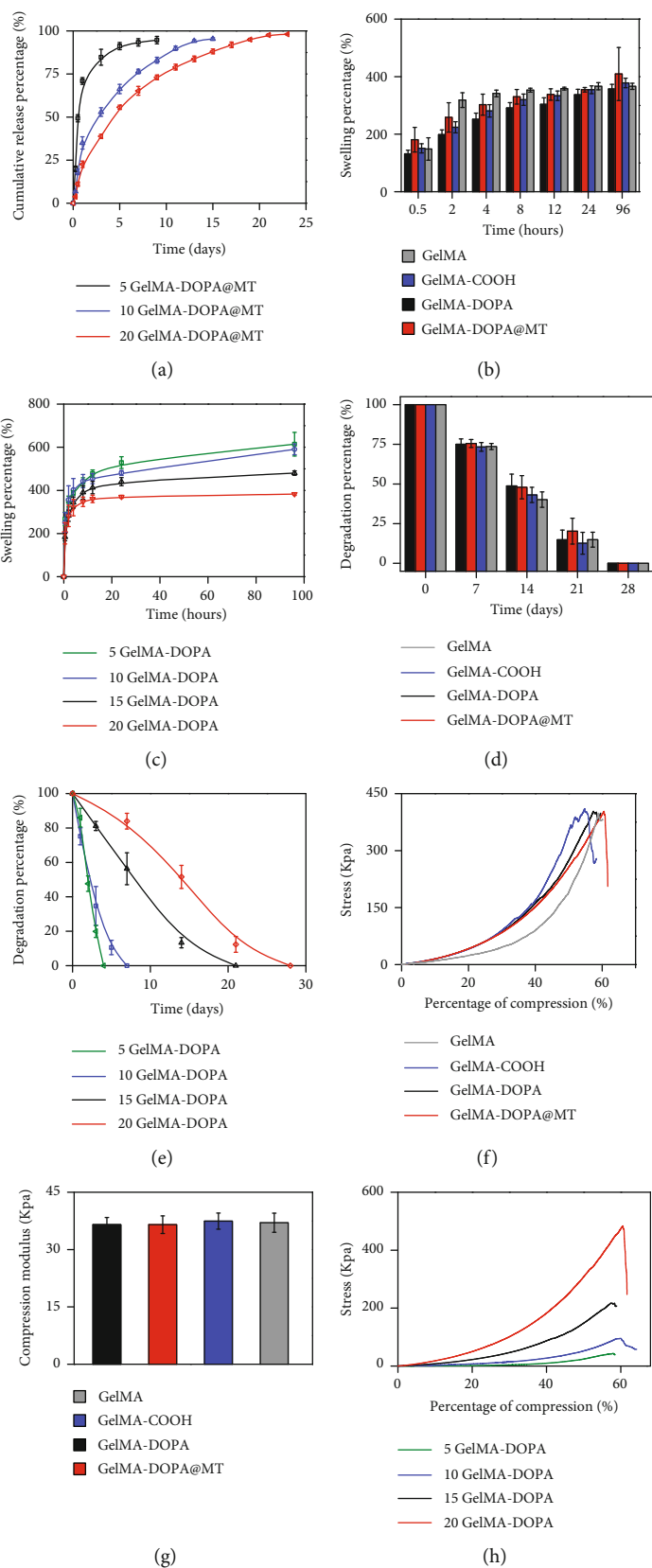


FIGURE 1: Continued.

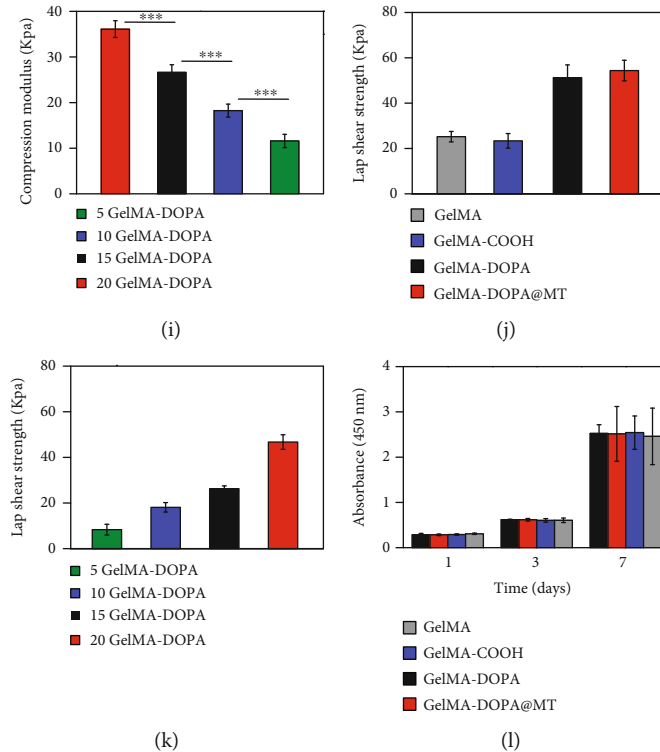


FIGURE 1: In vitro characterization of GelMA-DOPA@MT. (a) In vitro drug release behavior. (b) Swelling of GelMA with different modifications. (c) GelMA-DOPA at different concentrations. (d) Degradation of GelMA with different modifications. (e) GelMA-DOPA at different concentrations. (f, g) Compressive testing of GelMA with different modifications and Young's modulus. (h, i) Compressive testing on GelMA-DOPA at different concentrations and Young's modulus. (j, k) Investigation of the adhesive properties of GelMA-DOPA at different concentrations and Young's modulus. (l) Cytotoxicity of GelMA derivatives. ($n = 3$ per group, $*p < 0.05$, $**p < 0.01$, $***p < 0.001$).

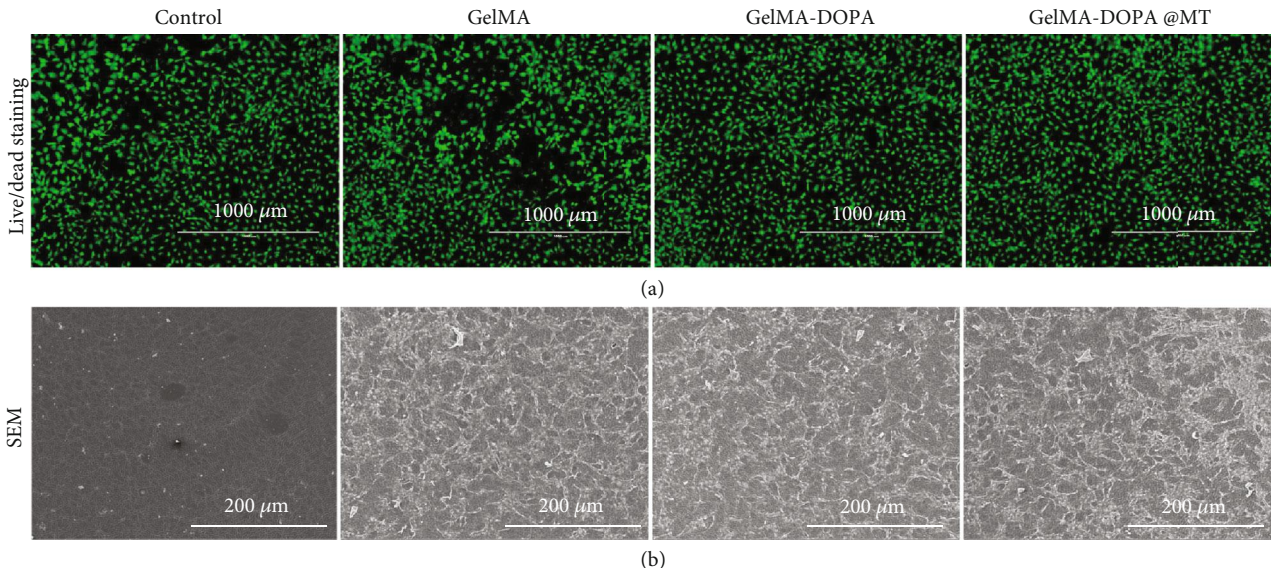
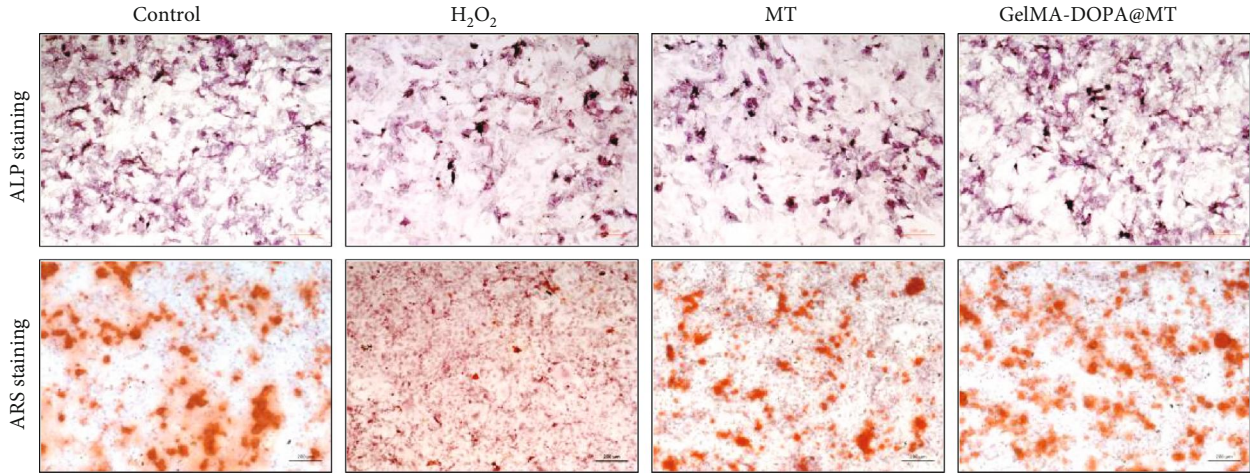


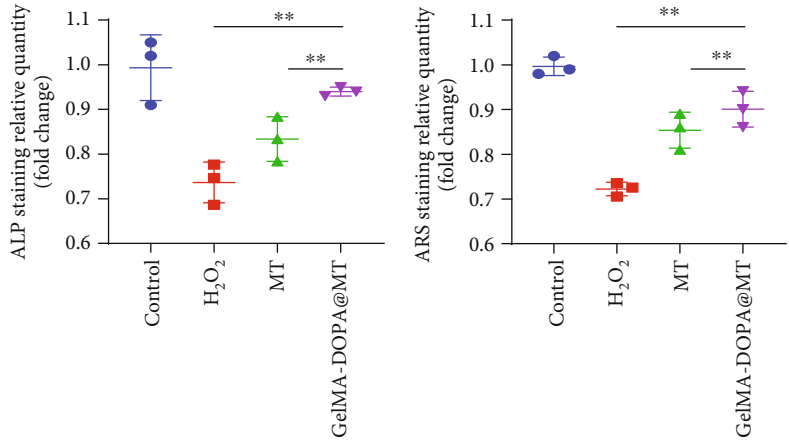
FIGURE 2: In vitro biocompatibility of GelMA-DOPA@MT. (a) Results of live/dead staining of MC3T3 cells cultured on the surfaces of GelMA derivatives. Scale bar: 1000 μm . (b) SEM imaging of MC3T3 cells cultured on the surfaces of GelMA derivatives. Scale bar: 200 μm .

Oxidative stress caused by H_2O_2 is often accompanied by cell apoptosis. We observed by TUNEL staining that H_2O_2 significantly increased apoptosis in MC3T3-E1 cells (Figure 4(a)), while the apoptosis of MC3T3-E1 cells in the MT and GelMA-DOPA@MT groups was inhibited. Quanti-

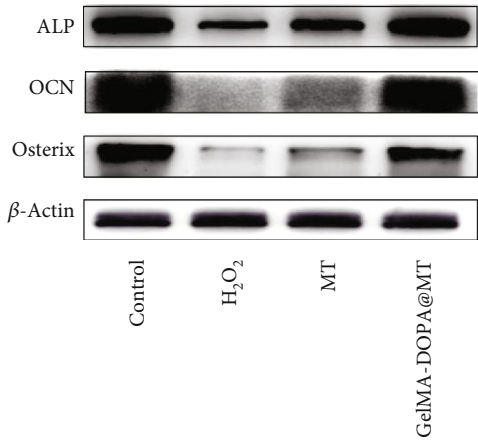
tative analysis (Figure 4(b)) showed that apoptosis in MC3T3-E1 cells in the GelMA-DOPA@MT group (0.8-fold) was decreased compared to that in MC3T3-E1 cells in the MT group. Further, Western blotting (Figures 4(c)–4(f)) also showed that H_2O_2 significantly increased the protein level of



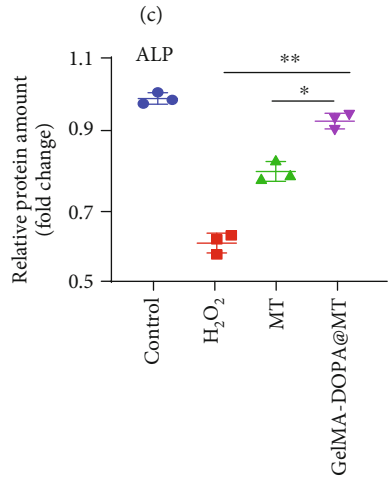
(a)



(b)



(d)



(e)

FIGURE 3: Continued.

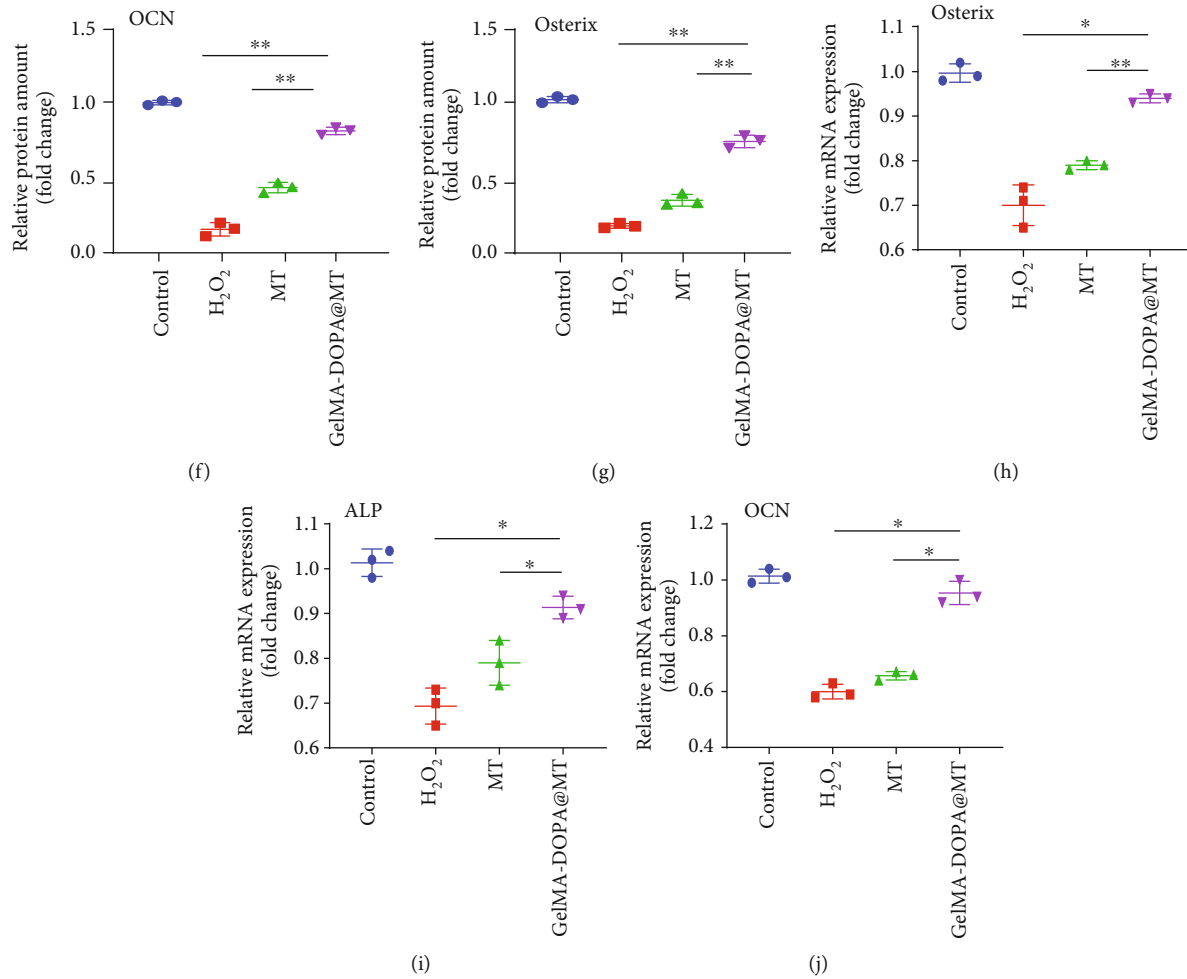


FIGURE 3: GelMA-DOPA@MT promotes the differentiation of osteoblasts in vitro. (a) Representative images showing ARS and ALP staining, with red and black arrows indicating calcium nodules. Scale bar: 50 μm . (b, c) Quantitative analysis of ARS and ALP staining. $n = 3$ per group, $*p < 0.05$, $**p < 0.01$, vs. the GelMA-DOPA@MT group. (d) Cell lysate was subjected to Western blotting with antibodies against the osteogenesis-specific proteins ALP, OCN, and Osterix. (e–g) Quantification of ALP, OCN, and Osterix protein levels, $n = 3$ per group, $*p < 0.05$, $**p < 0.01$, vs. the GelMA-DOPA@MT group. (h, i) qPCR analysis of the expression of the osteogenic genes ALP, OCN, and Osterix in the experimental group, $n = 3$ per group, $*p < 0.05$, $**p < 0.01$, vs. the GelMA-DOPA@MT group.

Bax and lowered the ratio of Bcl-2/Bax compared with those in the control group. Conversely, drug intervention reduced the Bax protein level and increased the ratio of Bcl-2/Bax, and the effects of drug intervention in the GelMA-DOPA@MT group were more obvious than those in the MT group. RT-PCR also showed similar results (Figures 4(g)–4(i)).

3.3. Effects of GelMA-DOPA@MT on the SIRT3/SOD2 Signaling Pathway. Previous research has shown that MT inhibits mitochondrial oxidative stress via the SIRT3/SOD2 signaling pathway. Because mitochondrial oxidative stress is an important factor in apoptosis, we focused on changes in SIRT3 in a mechanistic study. We first demonstrated the expression of SIRT3 in MC3T3-E1 cells by immunohistochemistry (IHC). As shown in Figures 5(a) and 5(b), H₂O₂ significantly reduced the expression of SIRT3, while drug intervention increased its expression, and SIRT3 activity in the GelMA-DOPA@MT group was significantly

higher than that in the MT group. We further evaluated the protein and gene expression levels of SIRT3 and SOD2 (Figures 5(c)–5(e)). As expected, H₂O₂ obviously decreased the protein level of SIRT3 and increased the ratio of Ac-SOD2/SOD2 compared to those in the control group. Conversely, drug intervention reversed this phenomenon. Meanwhile, the effect of MT on the GelMA-DOPA@MT group was more significant than that on the MT group.

A SIRT3-selective inhibitor (3-TYP) was used in the next experiment. TUNEL staining showed that the inhibitory effect of MT on apoptosis was inhibited by 3-TYP, and quantitative analysis showed that GelMA-DOPA@MT+3-TYP treatment did not effectively prevent the apoptosis of MC3T3-E1 cells in the GelMA-DOPA@MT+3-TYP group (by 2.5-fold) compared to that in the MT group (Figures 6(a) and 6(b)). Meanwhile, RT-PCR and Western blotting (Figures 6(c)–6(f)) confirmed that 3-TYP reversed the effective antiapoptotic effect of GelMA-DOPA@MT seen in the GelMA-DOPA@MT treatment group (RT: Bax, 2.1-fold; Bcl-2, 0.6-

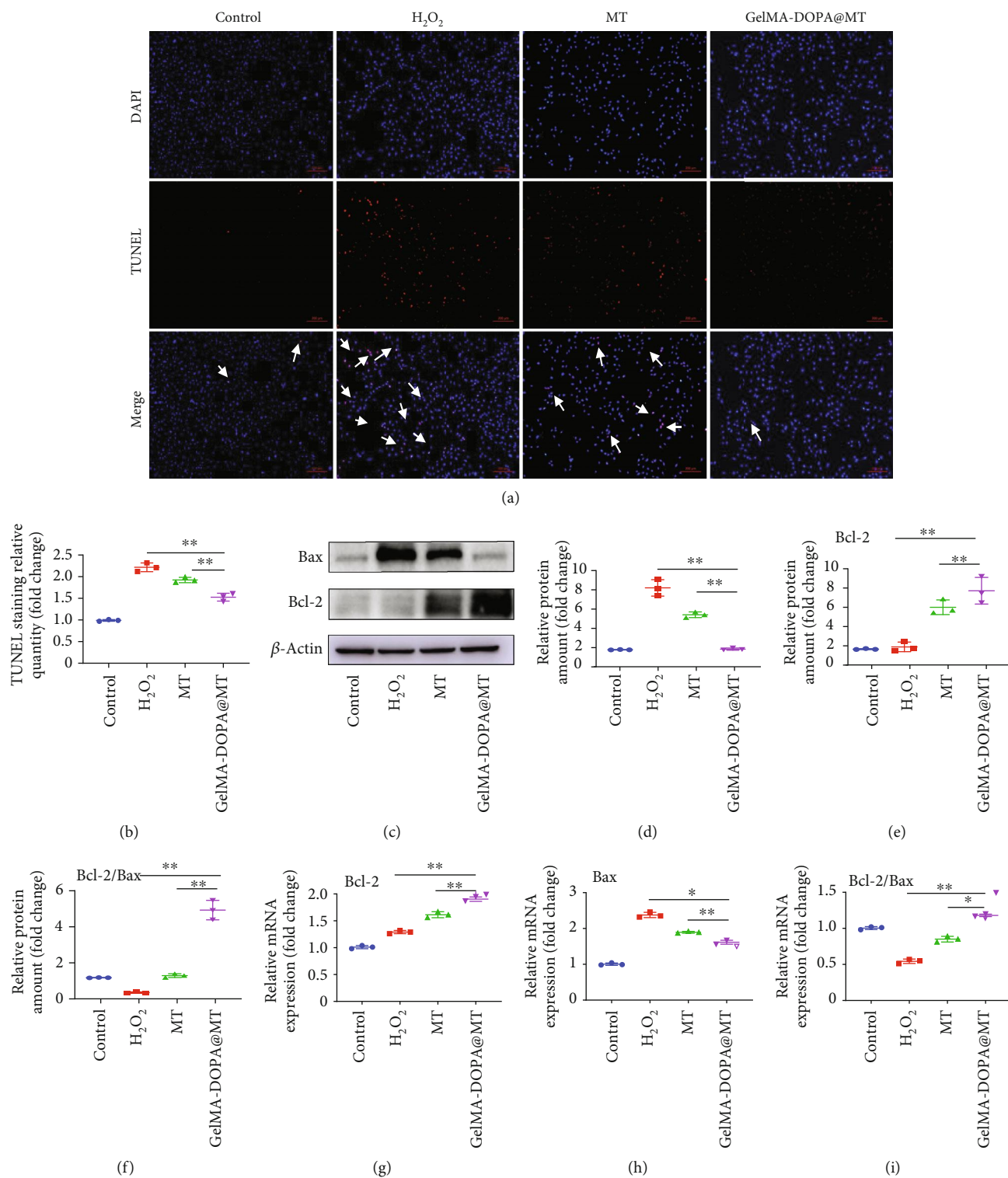


FIGURE 4: GelMA-DOPA@MT inhibits the apoptosis of osteoblasts in vitro. (a) Representative images showing TUNEL staining, with yellow arrows indicating apoptotic cells. Scale bar: 50 μm . (b) Quantitative analysis of TUNEL staining results. $n = 3$ per group, $*p < 0.05$, $**p < 0.01$, vs. the GelMA-DOPA@MT group. (c) Cell lysate was subjected to Western blotting with antibodies against the apoptosis-specific proteins Bax and Bcl-2. (d-f) Quantification of Bax and Bcl-2 protein levels, $n = 3$ per group, $*p < 0.05$, $**p < 0.01$, vs. the GelMA-DOPA@MT group. (g-i) qPCR analysis of the expression of the apoptosis-specific genes Bcl-2 and Bax in the experimental group. $n = 3$ per group, $*p < 0.05$, $**p < 0.01$, vs. the GelMA-DOPA@MT group.

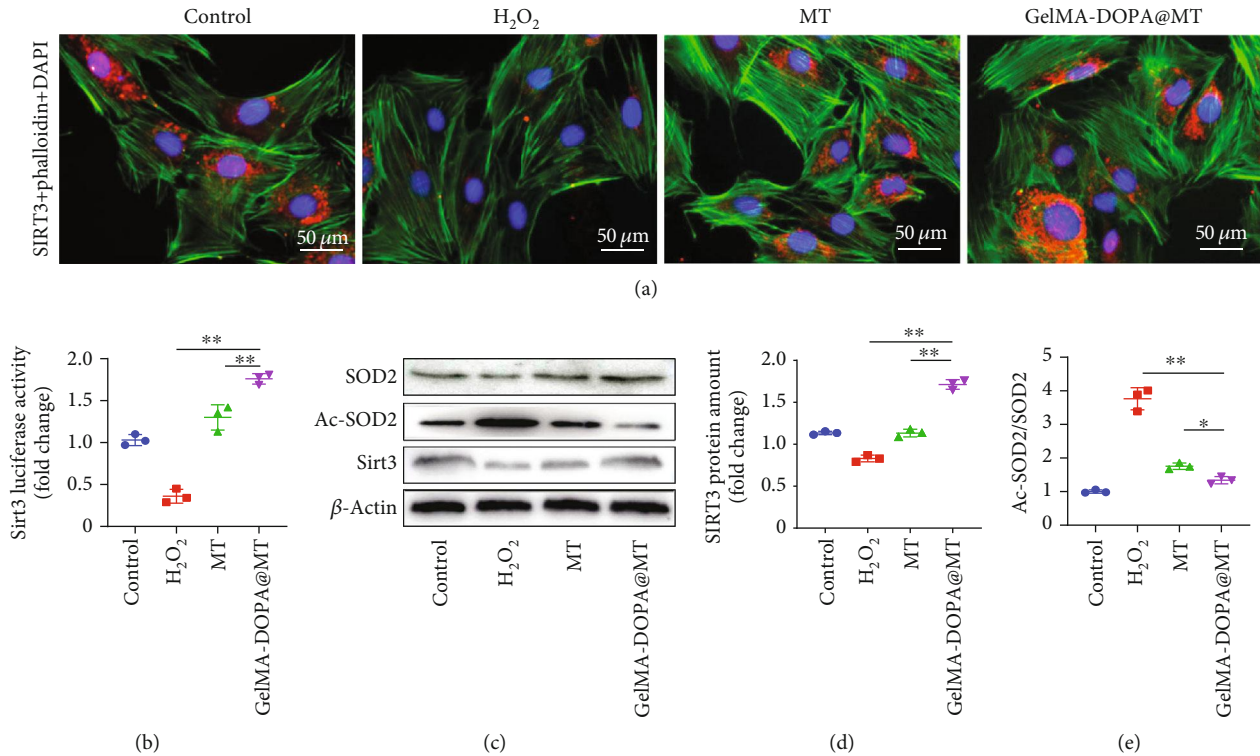


FIGURE 5: Effects of GelMA-DOPA@MT on the SIRT3/SOD2 signaling pathway. (a, b) Immunofluorescent staining for SIRT3 and quantitative analysis. Scale bar: 50 μm. $n = 3$ per group, $*p < 0.05$, $**p < 0.01$, vs. the GelMA-DOPA@MT group. (c) Western blotting of cell lysates with antibody against SIRT3, SOD2, and Ac-SOD2. (d) Quantitative analysis of SIRT3 protein levels and (e) the Ac-SOD2/SOD2 ratio in the experimental group, $n = 3$ per group, $*p < 0.05$, $**p < 0.01$, vs. the GelMA-DOPA@MT group.

fold) (Figures 6(g) and 6(i)). Finally, ALP and ARS staining showed that 3-TYP significantly inhibited ALP expression (by 0.5-fold vs. ALP expression in the GelMA-DOPA@MT group) and the formation of calcium nodules (by 0.4-fold vs. calcium nodule formation in the GelMA-DOPA@MT group) (Figures 7(a)–7(c)). RT-PCR and Western blotting further demonstrated that 3-TYP increased the expression of ALP and Osterix (RT: ALP, 0.6-fold; Osterix, 0.6-fold) (Figures 7(d)–7(h)).

3.4. GelMA-DOPA@MT Promotes Bone Mass around Ti Implants. Trabecular microstructures around the implanted Ti screws were also evaluated by 3D μ CT analysis (Figure 8(a)). Compared with that in the control group, the bone mass in the OVX group was significantly reduced, as shown by the following μ CT data: BMD (0.241 ± 0.007 vs. 0.151 ± 0.009 , respectively, g/cm^3), BV/TV (41.56 ± 1.14 vs. 26.03 ± 0.86 , respectively, %), BS/BV (29.36 ± 1.22 vs. 20.22 ± 1.29 , respectively, 1/mm), BS/TV (9.38 ± 0.56 vs. 7.39 ± 0.73 , respectively, 1/mm), and TbN (2.38 ± 0.07 vs. 1.92 ± 0.05 , respectively, 1/mm). However, after MT or GelMA-DOPA@MT was injected around the Ti screw, the bone mass increased, and the bone mass in the GelMA-DOPA@MT group was significantly greater than that in the MT group, as shown by the following μ CT data: BMD (0.225 ± 0.006 vs. 0.192 ± 0.006 , respectively, g/cm^3), BV/TV (37.13 ± 0.78 vs. 31.93 ± 0.87 , respectively, %), BS/BV (27.38 ± 1.14 vs. 22.42 ± 1.22 , respectively, 1/mm), BS/TV (9.09 ± 0.39 vs. 7.82 ± 0.32 , respectively, 1/mm), and TbN (2.28 ± 0.07 vs.

2.04 ± 0.10 , respectively, 1/mm) (Figures 8(d)–8(h)). These results indicated the presence of more trabecular bone around Ti screws in the GelMA-DOPA@MT-treated group than in the MT-treated group. Both groups exhibited more trabecular bone than the OVX group. In summary, the degree of bone formation around Ti screws in vivo was efficiently promoted by GelMA-DOPA@MT injection. Consistent with the μ CT results, histological analysis further confirmed the bone-protective effects of MT in osteoporotic rats. H&E staining of the surrounding tissues clearly showed fibrous capsule between the bone matrix and the Ti rod in the OVX- and GelMA-treated groups, indicating a significant inflammatory reaction induced by oxidative stress. In contrast, a more complete bone structure was observed in the MT- and GelMA-DOPA@MT-treated groups than that in the control group (Figure 8(b)). Single and double fluorochrome labeling, a direct histologic marker of bone formation, was more apparent, and the distance between double labels was shorter in the OVX group than in the control group, whereas GelMA-DOPA@MT treatment significantly increased single and double label interlabel width compared with that in the MT group (Figure 8(c)).

To further confirm the inhibitory effect of GelMA-DOPA@MT on apoptosis in osteoblasts in vivo, further study of the histological sections was performed by immunofluorescence staining. As shown in Figures 9(a)–9(f) and observed under confocal microscopy, the positive area in the OVX group was significantly larger than that in the control group, while in the MT-treated group, the positive area

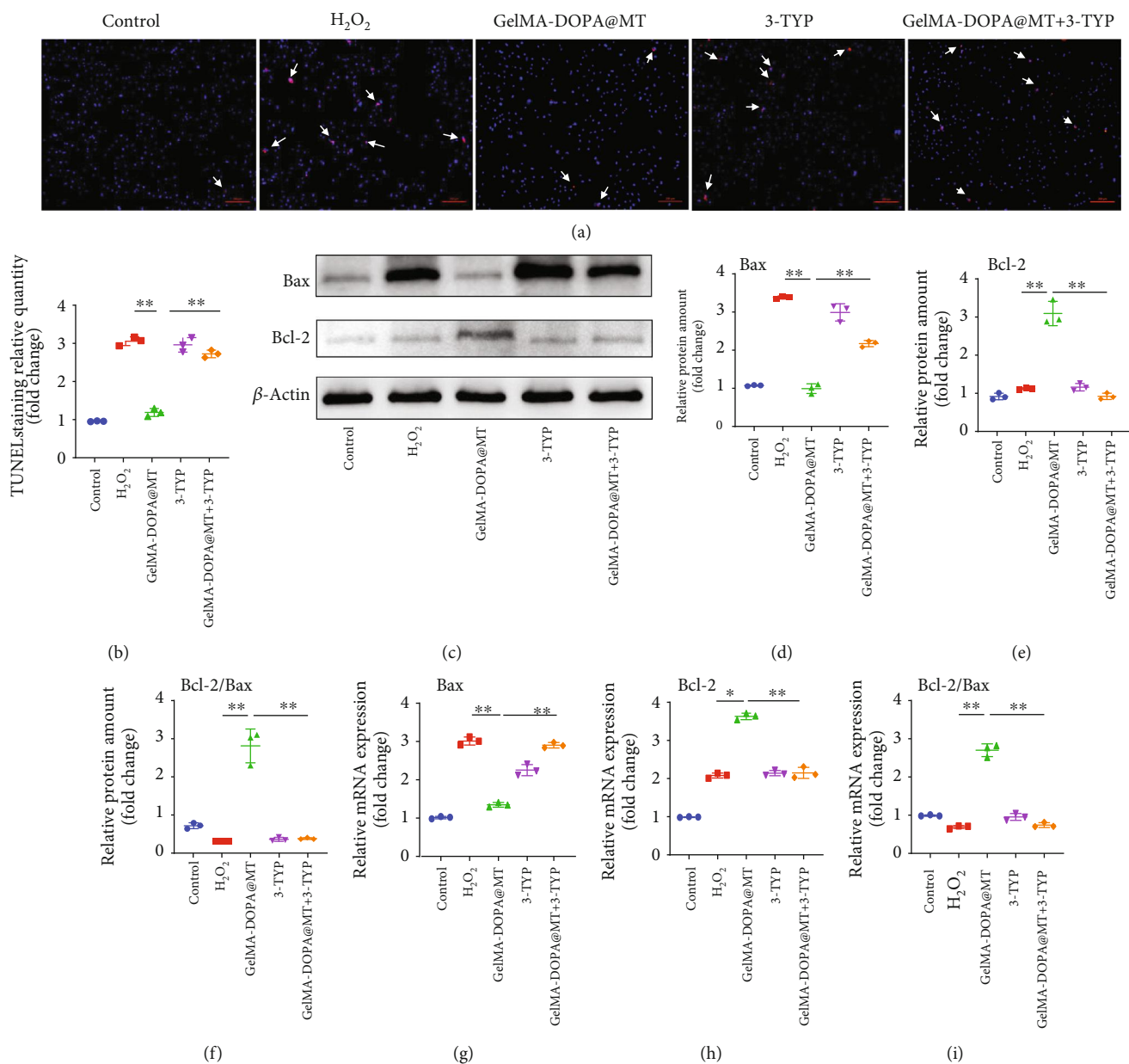


FIGURE 6: Melatonin inhibits osteoblast apoptosis by activating the sirt3 pathway and promotes osteogenic differentiation. (a, b) TUNEL staining and quantitative analysis, with yellow arrows indicating apoptotic cells. $n = 3$ per group, $*p < 0.05$, $**p < 0.01$, vs. the GelMA-DOPA@MT group. (c) Cell lysate was subjected to Western blotting with antibodies against the apoptosis-specific proteins Bax and Bcl-2. (d-f) Quantitative analysis of Bax and Bcl-2 protein levels, $n = 3$ per group, $*p < 0.05$, $**p < 0.01$, vs. the GelMA-DOPA@MT group. (g-i) qPCR analysis of the expression of the apoptosis-specific genes Bax and Bcl-2 in the experimental group, $n = 3$ per group, $*p < 0.05$, $**p < 0.01$, vs. the GelMA-DOPA@MT group.

was smaller than that in the OVX group, and the effect in the GelMA-DOPA@MT-treated group was more significant. These results confirmed that GelMA-DOPA@MT can effectively reduce the apoptosis of osteoblasts in vivo.

4. Discussion

Approximately 8.9 million fractures are caused by osteoporosis each year in the world. On average, one osteoporotic fracture occurs every 3 sec [41]. Osteoporosis will become a serious challenge for health authorities as many countries

in the world have an aging society [2, 3, 5]. Surgical treatment after fracture usually uses internal fixation to restore bone integrity and restore mechanical support. Internal fixation stability is an important factor for postoperative recovery from fractures [42]. Surgical treatment after fracture usually uses internal fixation to restore bone integrity and restore mechanical support. Internal fixation stability is an important factor for postoperative recovery from fractures [8, 43]. Importantly, we demonstrate that the apoptosis of osteoblasts may exacerbate deterioration due to osteoporosis and ultimately lead to loosening of the implant. Unfortunately,

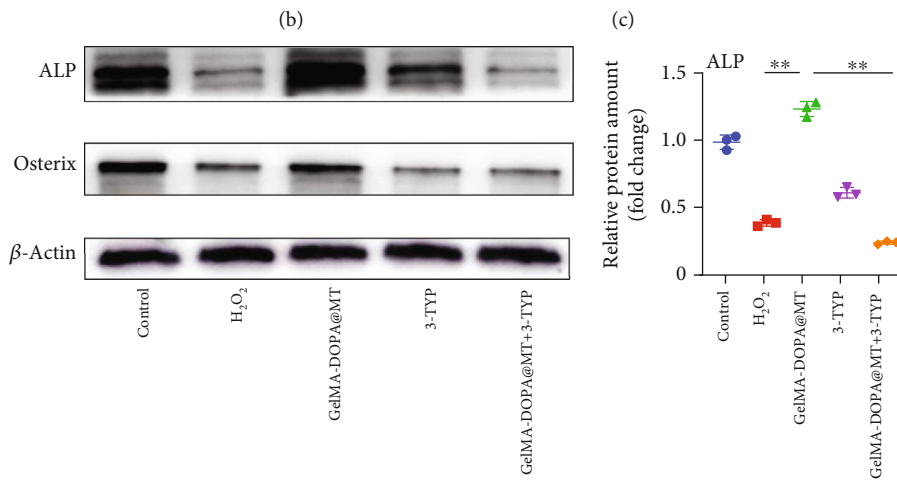
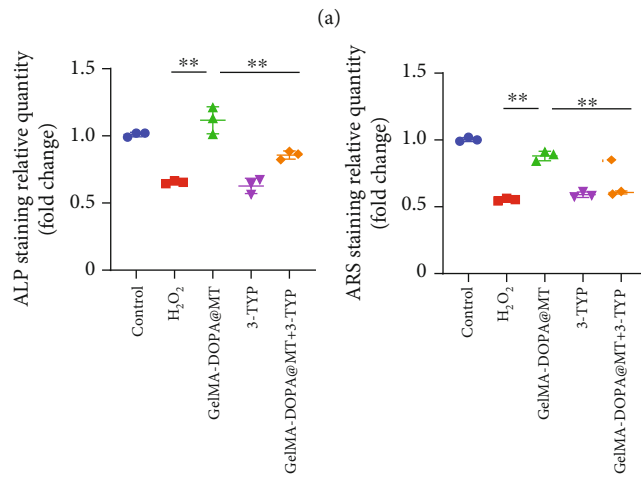
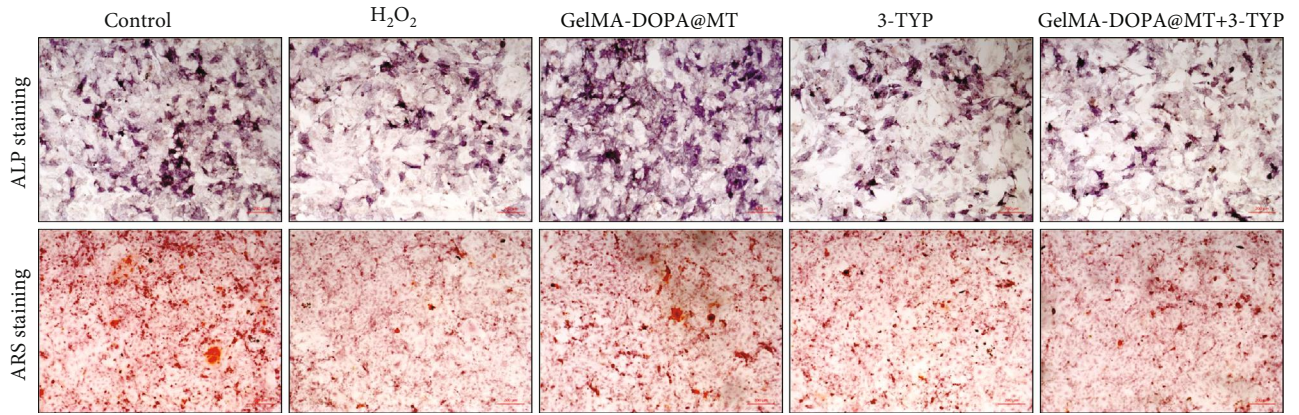


FIGURE 7: Continued.

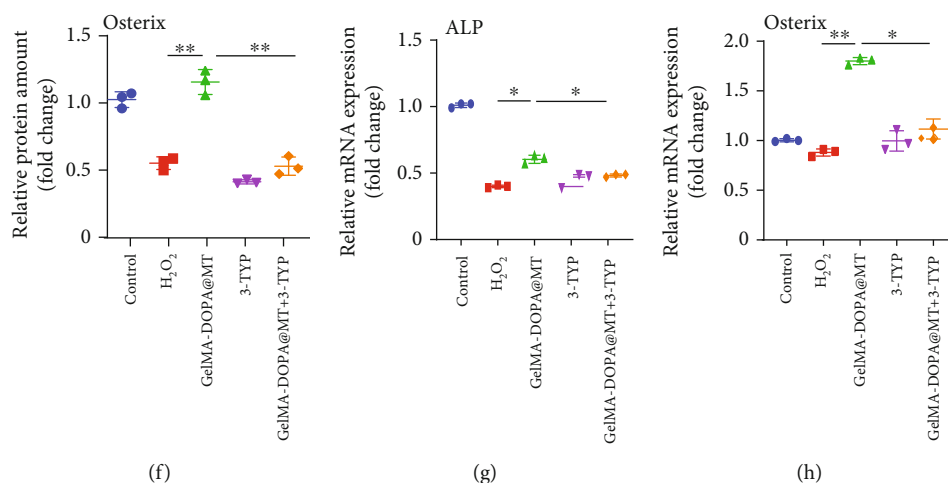


FIGURE 7: Melatonin promotes osteogenic differentiation by activating the sirt3 pathway. (a) Representative images showing cellular ARS and ALP staining. (b, c) Quantitative analysis of the results of ARS and ALP staining, $n = 3$ per group, $*p < 0.05$, $**p < 0.01$, vs. the GelMA-DOPA@MT group. (d) Cell lysate was subjected to Western blotting with antibodies against the osteogenesis-specific proteins ALP and Osterix. (e, f) Quantitative analysis of ALP and Osterix protein levels, $n = 3$ per group, $*p < 0.05$, $**p < 0.01$, vs. the GelMA-DOPA@MT group. (g, h) qPCR analysis of the expression of the osteogenesis-specific genes ALP and Osterix in the experimental group, $n = 3$ per group, $*p < 0.05$, $**p < 0.01$, vs. the GelMA-DOPA@MT group.

in patients with osteoporosis, there is no good method to protect the bone around the implant. Bone reconstruction is a dynamic process in which the homeostasis between bone resorption and bone formation is critical [44]. Importantly, we demonstrate that the apoptosis of osteoblasts may exacerbate deterioration due to osteoporosis and ultimately lead to loosening of the implant. Unfortunately, in patients with osteoporosis, there is no good method to protect the bone around the implant. Bone reconstruction is a dynamic process in which the homeostasis between bone resorption and bone formation is critical [45, 46]. In osteoporosis, the increased production of ROS may contribute significantly to the loss of bone around the implant [47]. Recently, an increasing number of studies have shown that oxidative stress-induced osteoblast apoptosis plays an important role in osteoporosis. These findings suggest that inhibiting osteoblast apoptosis can reduce the impact of osteoporosis [48].

MT, which is synthesized from serotonin in the human pineal gland, is involved in the regulation of many physiological processes, such as sleep induction and anti-inflammatory, antitumor, and antioxidant functions [20]. In recent years, the protective effect of MT on mitochondrial oxidative stress has been reported [28, 29, 49]. We studied the ability of GelMA-DOPA@MT extract to promote osteoblasts and inhibit osteoblast apoptosis in vitro. MT inhibited mitochondrial oxidative stress through the SIRT3 signaling pathway and attenuated the apoptosis of MC3T3-E1 osteoblasts. Sirtuins (SIRT3), a family of nicotinamide adenine dinucleotide- (NAD⁺) dependent deacetylases with seven members (SIRT1-SIRT7), among which SIRT1 and SIRT3 are the most extensively studied [50], have been shown to play an important role in apoptosis. SIRT3, a highly conserved NAD⁺-dependent deacetylase located in the mitochondria considered to be the most important acetyl lysine deacetylase, which regulates a variety of proteins to modulate mitochondrial effects and ROS production [51]. The role of mitochon-

drial oxidative stress has been widely confirmed. In our oxidative stress model, we observed a significant decrease in SIRT3 expression in MC3T3-E1 osteoblast precursor cells. MT increased SIRT3 expression and inhibited cell apoptosis compared to those in the H₂O₂ group. This effect of MT was significantly attenuated by a SIRT3-specific inhibitor. These results confirm the protective effect of MT on mitochondrial oxidative stress through the SIRT3 signaling pathway, reducing apoptosis-induced oxidative stress.

Studies in animals have shown that the systemic administration of MT enhances bone formation or integration [26, 52]. Orally and i.p. injected MT increased the volume of femoral cortical bones in mice. Similarly, Ostrowska et al. [53] found that i.p. injection of exogenous MT in rats following pineal gland resection inhibited biochemical markers of bone metabolism, such as ALP. Takechi et al. [54] reported that MT promoted osseointegration around tibial titanium implants in Wistar rats. Zhou et al. [55] showed that MT can accelerate bone formation around dental titanium implants. Therefore, the systemic administration of MT is a potential treatment for diseases such as osteoporosis that involve low bone density throughout the skeletal system. Similarly, studies by Calvoguirado et al. [56] have shown that the topical application of MT increases calcium deposition around implants. Furthermore, the cortical bone was regenerated around the width and length of tibial implants faster in rabbits that received topical MT than that in untreated rabbits. Therefore, topical MT administration induces bone healing without affecting other systems, which is often a powerful tool for treating local bone tissue.

However, the initial burst of MT release and short administration period are obvious shortcomings of the topical application of MT in bone repair and could limit the clinical application of MT to some extent. Therefore, it is especially necessary to establish a long-term drug delivery system for the local administration of MT. Liposomes have

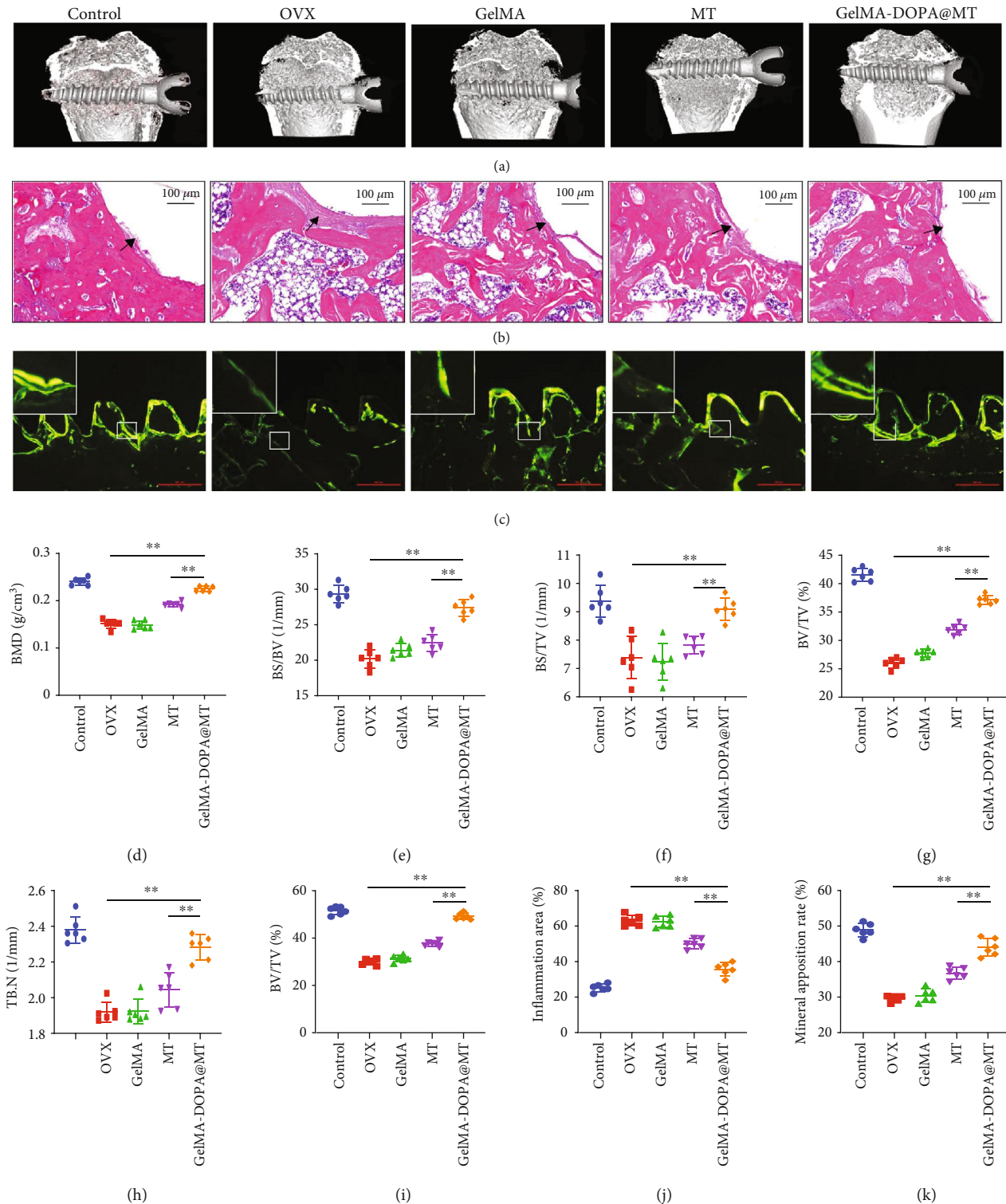


FIGURE 8: GelMA-DOPA@MT prevents ovariectomy- (OVX-) induced bone loss in vivo. (a) Representative 3D reconstructions of μ CT images and (d) BMD within the ROI (region of interest) were calculated. (e) BS/BV, (f) BS/TV, (g) BV/TV, and (h) TbN. (b) Representative paraffinized section following H&E staining. Black arrows represent inflammatory fibrous tissue, Scale bar: 100 μ m. (c) Representative histological images around the screw showing calcein levels. Scale bar: 500 μ m. (i) BV/TV and (j) inflammatory area. (k) Mineral apposition rate. $n = 6$ per group, $*p < 0.05$, $**p < 0.01$, vs. the GelMA-DOPA@MT group.

been used as FDA-approved drug carriers to control drug release for several decades [57]. Additionally, due to their bilayer structure, liposomes can effectively carry both hydro-

philic and hydrophobic drugs [34, 35]. However, it is difficult to maintain a certain therapeutic drug concentration during liquid administration. GelMA-DOPA, a gelatin derivative,

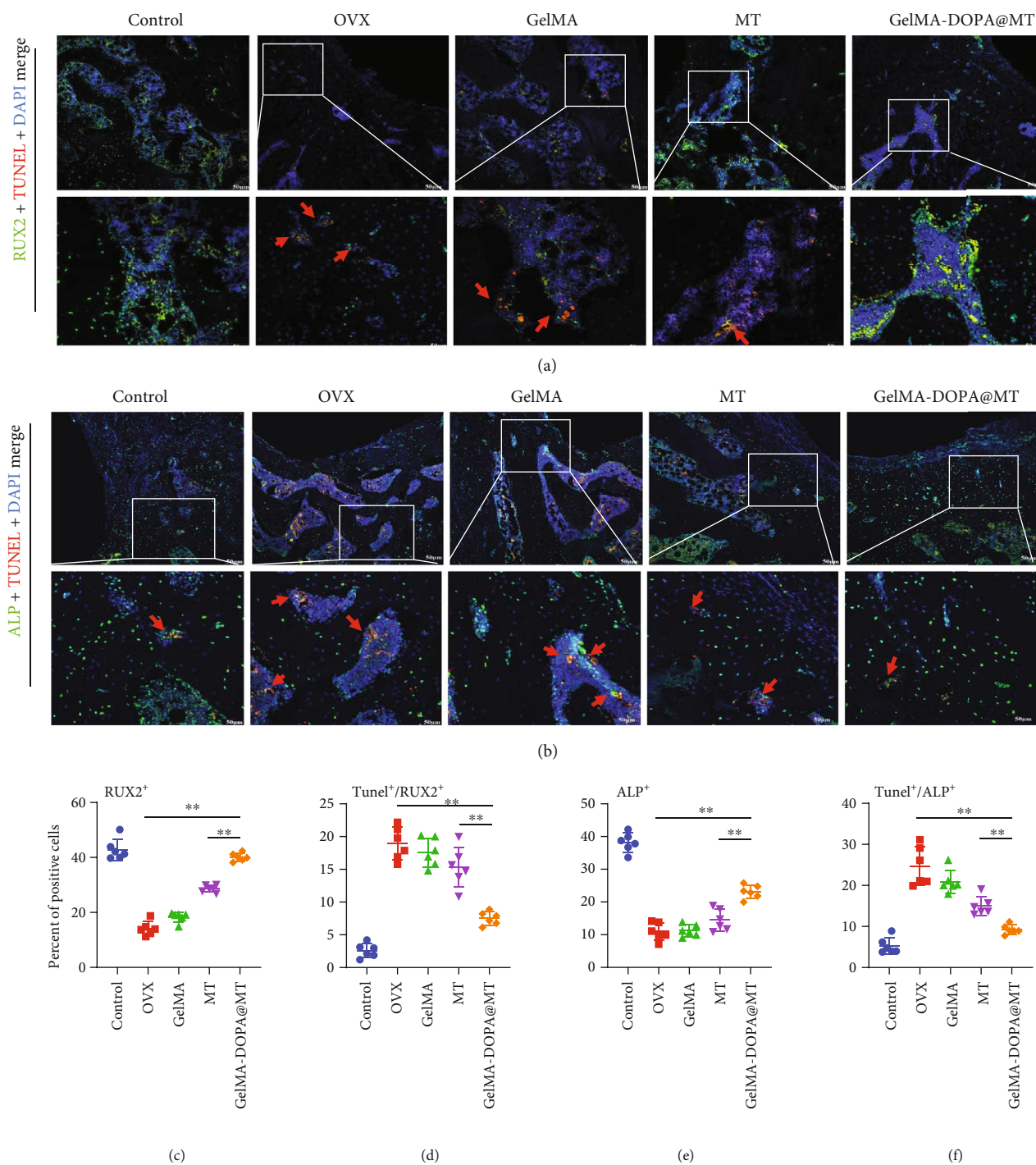


FIGURE 9: Fluorescence staining of tissue sections was used to analyze the effect of GelMA-DOPA@MT on osteoblast apoptosis around the implant. (a) Representative images showing cells stained for the osteogenic gene RUX2 (green), apoptosis (red), and nuclei (blue) observed by confocal microscopy. (b) Representative images showing cells stained for the osteogenic gene ALP (green), apoptosis (red), and nuclei (blue) observed by confocal microscopy. The red arrow indicates the apoptotic region during osteogenesis. Scale bar: 50 μm . (c) Percent of positive cells of RNX2. (d) Ratio of TUNel/RUX2. (e) Percent of positive cells of ALP. (f) Ratio of TUNel/ALP. $n = 6$ per group, $*p < 0.05$, $**p < 0.01$, vs. the GelMA-DOPA@MT group.

shows satisfactory adhesive properties, biodegradability, and biocompatibility [31–33]. Before its exposure to UV light, a precrosslinked GelMA solution could be injected and used to fill the gap between the implant and the cancellous bone [58]. After crosslinking, a complete amalgam between the

implant and bone is generated. In this study, we prepared MT liposomes (MT@liposomes), which were then mixed with a GelMA-DOPA solution to prepare a precrosslinked solution. Then, the solution was injected into the bone defect area, followed by its exposure to UV light. Finally, a sustained

MT release system with favorable adhesive properties to join implants and the surrounding tissues was generated.

Nevertheless, there were several limitations in this study. On the one hand, as we all know, bone metabolism includes both bone formation and bone resorption. However, our results only showed that GelMA-DOPA@MT increased bone mass around Ti screws through promotion of bone formation. Although Ping et al. [59] demonstrated that MT inhibits bone resorption at osteolytic sites caused by titanium particle-stimulation, whether GelMA-DOPA@MT can affect bone resorption around Ti screws requires further research. This question is currently the focus of ongoing study in our laboratory. On the other hand, the OVX-induced osteoporosis model applied in our study is different from osteoporosis with natural aging. Regardless of human or animals, age can affect the number, proliferation, and differentiation of cells [60, 61]. Therefore, the aging osteoporosis model which was more clinically relevant is necessary to verify the effect of GelMA-DOPA@MT on the stability of implants. Additionally, we need to use human-derived osteoblasts, osteoclasts, or human cell lines to further make it more clinically relevant in the following experiments.

5. Conclusion

In this study, we developed a novel MT sustained release system, GelMA-DOPA@MT, which can attach to the surface of Ti screws by photocrosslinked under UV light. In addition, GelMA-DOPA@MT can suppress osteoblast apoptosis induced by oxidative stress, thereby promoting osteogenic differentiation and improving bone quality around the prosthesis through activating the SIRT3/SOD2 signaling pathway. This system of local, sustained MT release is a suitable candidate for the treatment of implant loosening in patients with osteoporosis.

Data Availability

The data used to support the findings of this study are available from the corresponding author upon request.

Conflicts of Interest

The authors declare no competing financial interest.

Authors' Contributions

The manuscript was written through contributions of all authors. All authors have given approval to the final version of the manuscript. Long Xiao and Jiayi Lin contributed equally.

Acknowledgments

We greatly acknowledge the financial support from the National Natural Science Foundation of China (81873990, 81873991, and 81672238), the Natural Science Foundation of Jiangsu province (BK20180001 and BK20191201), Suzhou Science and Technology Development Plan Project (SYS2017008, SYS2018001, and SYS2018003), the Suzhou Science and

Education Technology Project (KJXW2017061 and KJXW2018058), the Suzhou Health Personnel Training Project (GSWS2019074), the Zhangjiagang Health System Youth Science and Technology Project (ZJGQNKJ201804, ZJGQNKJ201807) and the 2019 National Teacher System Training Project for Young Health Talents of Suzhou.

Supplementary Materials

Figure S1: GelMA-DOPA@MT promotes the differentiation of osteoblasts in vitro (BMSC). Table S1: the quantitative results of CCK8 staining. (*Supplementary materials*)

References

- [1] S. D. Berry, S. Shi, and D. P. Kiel, "Considering the risks and benefits of osteoporosis treatment in older adults," *JAMA Internal Medicine*, vol. 179, no. 8, p. 1103, 2019.
- [2] J. E. Compston, M. R. McClung, and W. D. Leslie, "Osteoporosis," *The Lancet*, vol. 393, no. 10169, pp. 364–376, 2019.
- [3] S. Khosla and L. C. Hofbauer, "Osteoporosis treatment: recent developments and ongoing challenges," *The Lancet Diabetes & Endocrinology*, vol. 5, no. 11, pp. 898–907, 2017.
- [4] N. Harvey, E. Dennison, and C. Cooper, "Osteoporosis: a life-course approach," *Journal of Bone and Mineral Research*, vol. 29, no. 9, pp. 1917–1925, 2014.
- [5] S. D. Berry, D. P. Kiel, and C. Colon-Emeric, "Hip fractures in older adults in 2019," *JAMA*, vol. 321, no. 22, pp. 2231–2232, 2019.
- [6] R. Bartl and B. Frisch, "Periprosthetic osteoporosis and aseptic loosening of prostheses, in osteoporosis: diagnosis, prevention, therapy," in *Osteoporosis*, pp. 247–250, Springer Science & Business Media, Berlin, Heidelberg, 2009.
- [7] H. S. Alghamdi, R. Bosco, S. K. Both et al., "Synergistic effects of bisphosphonate and calcium phosphate nanoparticles on peri-implant bone responses in osteoporotic rats," *Biomaterials*, vol. 35, no. 21, pp. 5482–5490, 2014.
- [8] A. Temmerman, L. Rasmusson, A. Kübler, A. Thor, J. Merheb, and M. Quirynen, "A prospective, controlled, multicenter study to evaluate the clinical outcome of implant treatment in women with osteoporosis/osteopenia: 5-year results," *Journal of Dental Research*, vol. 98, no. 1, pp. 84–90, 2018.
- [9] J. Merheb, A. Temmerman, L. Rasmusson, A. Kübler, A. Thor, and M. Quirynen, "Influence of skeletal and local bone density on dental implant stability in patients with osteoporosis," *Clinical Implant Dentistry and Related Research*, vol. 18, no. 2, pp. 253–260, 2016.
- [10] G. Alsaadi, M. Quirynen, A. Komárek, and D. Van Steenberghe, "Impact of local and systemic factors on the incidence of oral implant failures, up to abutment connection," *Journal of Clinical Periodontology*, vol. 34, no. 7, pp. 610–617, 2007.
- [11] N. M. Desy and M. P. Abdel, *Aseptic implant loosening, in complications after primary total hip arthroplasty*, M. Abdel and V. C. Della, Eds., Springer, Cham, 2017.
- [12] A. Stavropoulos, K. Bertl, P. Pietschmann, N. Pandis, M. Schiødt, and B. Klinge, "The effect of antiresorptive drugs on implant therapy: systematic review and meta-analysis," *Clinical Oral Implants Research*, vol. 29, Suppl 18, pp. 54–92, 2018.
- [13] L. Shi, L. Wang, Y. Zhang et al., "Improving fixation strength of pedicle screw by microarc oxidation treatment: an

- experimental study of osteoporotic spine in sheep,” *Journal of Orthopaedic Research*, vol. 30, no. 8, pp. 1296–1303, 2012.
- [14] L. Zhang, Y. Pang, Y. Shi et al., “Indirect comparison of teriparatide, denosumab, and oral bisphosphonates for the prevention of vertebral and nonvertebral fractures in postmenopausal women with osteoporosis,” *Menopause*, vol. 22, no. 9, pp. 1021–1025, 2015.
- [15] L. Chow, T. W. Chow, J. Chai, and N. Mattheos, “Bone stability around implants in elderly patients with reduced bone mineral density - a prospective study on mandibular overdentures,” *Clinical Oral Implants Research*, vol. 28, no. 8, pp. 966–973, 2017.
- [16] P. Taxel, D. Ortiz, D. Shafer et al., “The relationship between implant stability and bone health markers in postmenopausal women with bisphosphonate exposure,” *Clinical Oral Investigations*, vol. 18, no. 1, pp. 49–57, 2014.
- [17] H. Dagaard, B. Elmengaard, T. T. Andreassen, A. Lamberg, J. E. Bechtold, and K. Soballe, “Systemic intermittent parathyroid hormone treatment improves osseointegration of press-fit inserted implants in cancellous bone,” *Acta Orthopaedica*, vol. 83, no. 4, pp. 411–419, 2012.
- [18] M. S. R. Aziz, B. Nicayenzi, M. C. Crookshank, H. Bougherara, E. H. Schemitsch, and R. Zdero, “Biomechanical measurements of cortical screw purchase in five types of human and artificial humeri,” *Journal of the Mechanical Behavior of Biomedical Materials*, vol. 30, pp. 159–167, 2014.
- [19] S.-y. Wan, Z.-x. Wu, W. Zhang et al., “Expandable pedicle screw trajectory in cadaveric lumbar vertebra,” *Journal of Spinal Disorders & Techniques*, vol. 24, no. 5, pp. 313–317, 2011.
- [20] S. R. Pandi-Perumal, V. Srinivasan, G. J. M. Maestroni, D. P. Cardinali, B. Poegeleler, and R. Hardeland, “Melatonin,” *FEBS Journal*, vol. 273, no. 13, pp. 2813–2838, 2006.
- [21] C.-C. Chang, T. Y. Huang, H. Y. Chen et al., “Protective effect of melatonin against oxidative stress-induced apoptosis and enhanced autophagy in human retinal pigment epithelium cells,” *Oxidative Medicine and Cellular Longevity*, vol. 2018, 12 pages, 2018.
- [22] B. I. Fernandez-Gil, A. Guerra-Librero, Y. Q. Shen et al., “Melatonin enhances cisplatin and radiation cytotoxicity in head and neck squamous cell carcinoma by stimulating mitochondrial ROS generation, apoptosis, and autophagy,” *Oxidative Medicine and Cellular Longevity*, vol. 2019, 12 pages, 2019.
- [23] G. H. Tamarindo, D. L. Ribeiro, M. G. Gobbo et al., “Melatonin and docosahexaenoic acid decrease proliferation of PNT1A prostate benign cells via modulation of mitochondrial bioenergetics and ROS production,” *Oxidative Medicine and Cellular Longevity*, vol. 2019, 15 pages, 2019.
- [24] S. Ma, J. Chen, J. Feng et al., “Melatonin ameliorates the progression of atherosclerosis via mitophagy activation and NLRP3 inflammasome inhibition,” *Oxidative Medicine and Cellular Longevity*, vol. 2018, 12 pages, 2018.
- [25] X.-F. Hu, L. Wang, G. Xiang, W. Lei, and Y. F. Feng, “Angiogenesis impairment by the NADPH oxidase-triggered oxidative stress at the bone-implant interface: critical mechanisms and therapeutic targets for implant failure under hyperglycemic conditions in diabetes,” *Acta Biomaterialia*, vol. 73, pp. 470–487, 2018.
- [26] J.-L. Calvo-Guirado, G. Gómez-Moreno, J.-E. Maté-Sánchez, L. López-Marí, R. Delgado-Ruiz, and G. E. Romanos, “Retracted: New bone formation in bone defects after melatonin and porcine bone grafts: experimental study in rabbits,” *Clinical Oral Implants Research*, vol. 26, no. 4, pp. 399–406, 2015.
- [27] S. Maria and P. A. Witt-Enderby, “Melatonin effects on bone: potential use for the prevention and treatment for osteopenia, osteoporosis, and periodontal disease and for use in bone-grafting procedures,” *Journal of Pineal Research*, vol. 56, no. 2, pp. 115–125, 2014.
- [28] S. Proksch, S. L. Strobel, K. Vach et al., “Melatonin as a candidate therapeutic drug for protecting bone cells from chlorhexidine-induced damage,” *Journal of Periodontology*, vol. 85, no. 12, pp. e379–e389, 2014.
- [29] C. Luo, Q. Yang, Y. Liu et al., “The multiple protective roles and molecular mechanisms of melatonin and its precursor N-acetylserotonin in targeting brain injury and liver damage and in maintaining bone health,” *Free Radical Biology & Medicine*, vol. 130, pp. 215–233, 2019.
- [30] H. Balci Yuce, O. Karatas, H. Aydemir Turkal et al., “The effect of melatonin on bone loss, diabetic control, and apoptosis in rats with diabetes with ligature-induced periodontitis,” *Journal of Periodontology*, vol. 87, no. 4, pp. e35–e43, 2016.
- [31] W. Schuurman, P. A. Levett, M. W. Pot et al., “Gelatin-methacrylamide hydrogels as potential biomaterials for fabrication of tissue-engineered cartilage constructs,” *Macromolecular Bioscience*, vol. 13, no. 5, pp. 551–561, 2013.
- [32] M. Kéri, A. Forgács, V. Papp et al., “Gelatin content governs hydration induced structural changes in silica-gelatin hybrid aerogels – Implications in drug delivery,” *Acta Biomaterialia*, vol. 105, pp. 131–145, 2020.
- [33] D. Ma, Y. Zhao, L. Huang et al., “A novel hydrogel-based treatment for complete transection spinal cord injury repair is driven by microglia/macrophages repopulation,” *Biomaterials*, vol. 237, p. 119830, 2020.
- [34] A. Haeri, S. Sadeghian, S. Rabbani et al., “Effective attenuation of vascular restenosis following local delivery of chitosan decorated sirolimus liposomes,” *Carbohydrate Polymers*, vol. 157, pp. 1461–1469, 2017.
- [35] C. Liu, K. K. Ewert, N. Wang, Y. Li, C. R. Safinya, and W. Qiao, “A multifunctional lipid that forms contrast-agent liposomes with dual-control release capabilities for precise MRI-guided drug delivery,” *Biomaterials*, vol. 221, p. 119412, 2019.
- [36] R. Cheng, Y. Yan, H. Liu et al., “Mechanically enhanced lipohydrogel with controlled release of multi-type drugs for bone regeneration,” *Applied Materials Today*, vol. 12, pp. 294–308, 2018.
- [37] K. Yue, G. Trujillo-de Santiago, M. M. Alvarez, A. Tamayol, N. Annabi, and A. Khademhosseini, “Synthesis, properties, and biomedical applications of gelatin methacryloyl (GelMA) hydrogels,” *Biomaterials*, vol. 73, pp. 254–271, 2015.
- [38] H. Cheng, K. Yue, M. Kazemzadeh-Narbat et al., “Mussel-inspired multifunctional hydrogel coating for prevention of infections and enhanced osteogenesis,” *ACS Applied Materials & Interfaces*, vol. 9, no. 13, pp. 11428–11439, 2017.
- [39] X. Zhao, Q. Lang, L. Yildirimer et al., “Photocrosslinkable gelatin hydrogel for epidermal tissue engineering,” *Advanced Healthcare Materials*, vol. 5, no. 1, pp. 108–118, 2016.
- [40] T. Xin, Y. Gu, R. Cheng et al., “Inorganic strengthened hydrogel membrane as regenerative periosteum,” *ACS Applied Materials & Interfaces*, vol. 9, no. 47, pp. 41168–41180, 2017.
- [41] O. Johnell and J. A. Kanis, “An estimate of the worldwide prevalence and disability associated with osteoporotic fractures,” *Osteoporosis International*, vol. 17, no. 12, pp. 1726–1733, 2006.

- [42] R. S. Zhu et al., "Biomechanical stability of pedicle screw in spine internal fixation," *Chin. J. Tissue Eng. Res.*, 2013.
- [43] L. Wang, X. Guo, W. Zhou et al., "Protein phosphatase 2A as a new target for downregulating osteoclastogenesis and alleviating titanium particle-induced bone resorption," *Acta Biomaterialia*, vol. 73, pp. 488–499, 2018.
- [44] N. C. Walsh and E. M. Gravallese, "Bone remodeling in rheumatic disease: a question of balance," *Immunological Reviews*, vol. 233, no. 1, pp. 301–312, 2010.
- [45] D. J. Hunter and S. Bierma-Zeinstra, "Osteoarthritis," *The Lancet*, vol. 393, no. 10182, pp. 1745–1759, 2019.
- [46] M. B. Greenblatt, J. N. Tsai, and M. N. Wein, "Bone turnover markers in the diagnosis and monitoring of metabolic bone disease," *Clinical Chemistry*, vol. 63, no. 2, pp. 464–474, 2017.
- [47] S. A. Sheweta, K. I. Khoshhal, and H. H. Baghdadi, *Osteoporosis and oxidative stress – role of antioxidants, in systems biology of free radicals and antioxidants*, I. Laher, Ed., Springer-Verlag, Berlin, Heidelberg, 2014.
- [48] P. Dai, Y. Mao, X. Sun et al., "Attenuation of oxidative stress-induced osteoblast apoptosis by curcumin is associated with preservation of mitochondrial functions and increased Akt-GSK3 β signaling," *Cellular Physiology and Biochemistry*, vol. 41, no. 2, pp. 661–677, 2017.
- [49] D. Bandyopadhyay, K. Biswas, U. Bandyopadhyay, R. J. Reiter, and R. K. Banerjee, "Melatonin protects against stress-induced gastric lesions by scavenging the hydroxyl radical," *Journal of Pineal Research*, vol. 29, no. 3, pp. 143–151, 2000.
- [50] E. Verdin, M. D. Hirschey, L. W. S. Finley, and M. C. Haigis, "Sirtuin regulation of mitochondria: energy production, apoptosis, and signaling," *Trends in Biochemical Sciences*, vol. 35, no. 12, pp. 669–675, 2010.
- [51] Y. Ding, H. Yang, Y. Wang, J. Chen, Z. Ji, and H. Sun, "Sirtuin 3 is required for osteogenic differentiation through maintenance of PGC-1 α -SOD2-mediated regulation of mitochondrial function," *International Journal of Biological Sciences*, vol. 13, no. 2, pp. 254–264, 2017.
- [52] A. K. Amstrup, T. Sikjaer, L. Heickendorff, L. Mosekilde, and L. Rejnmark, "Melatonin improves bone mineral density at the femoral neck in postmenopausal women with osteopenia: a randomized controlled trial," *Journal of Pineal Research*, vol. 59, no. 2, pp. 221–229, 2015.
- [53] Z. Ostrowska, B. Kos-Kudla, M. Nowak et al., "The relationship between bone metabolism, melatonin and other hormones in sham-operated and pinealectomized rats," *Endocrine Regulations*, vol. 37, no. 4, pp. 211–224, 2003.
- [54] M. Takechi, S. Tatehara, K. Satomura, K. Fujisawa, and M. Nagayama, "Effect of FGF-2 and melatonin on implant bone healing: a histomorphometric study," *Journal of Materials Science. Materials in Medicine*, vol. 19, no. 8, pp. 2949–2952, 2008.
- [55] W. Zhou, Y. Liu, J. Shen et al., "Melatonin increases bone mass around the prostheses of OVX rats by ameliorating mitochondrial oxidative stress via the SIRT3/SOD2 signaling pathway," *Oxidative Medicine and Cellular Longevity*, vol. 2019, 16 pages, 2019.
- [56] J. L. Calvo-Guirado, G. Gómez-Moreno, L. López-Marí et al., "Actions of melatonin mixed with collagenized porcine bone versus porcine bone only on osteointegration of dental implants," *Journal of Pineal Research*, vol. 48, no. 3, pp. 194–203, 2010.
- [57] S. S. Liow, Q. Dou, D. Kai et al., "Long-term real-time in vivo drug release monitoring with AIE thermogelling polymer," *Small*, vol. 13, no. 7, p. 1603404, 2017.
- [58] P. Chen, C. Xia, S. Mei et al., "Intra-articular delivery of sinomenium encapsulated by chitosan microspheres and photo-crosslinked GelMA hydrogel ameliorates osteoarthritis by effectively regulating autophagy," *Biomaterials*, vol. 81, pp. 1–13, 2016.
- [59] Z. Ping, Z. Wang, J. Shi et al., "Inhibitory effects of melatonin on titanium particle-induced inflammatory bone resorption and osteoclastogenesis via suppression of NF- κ B signaling," *Acta Biomaterialia*, vol. 62, pp. 362–371, 2017.
- [60] J. C. Ra, S. K. Kang, I. S. Shin et al., "Stem cell treatment for patients with autoimmune disease by systemic infusion of culture-expanded autologous adipose tissue derived mesenchymal stem cells," *Journal of Translational Medicine*, vol. 9, no. 1, 2011.
- [61] H. Y. Liu, J. F. Chiou, A. T. H. Wu et al., "The effect of diminished osteogenic signals on reduced osteoporosis recovery in aged mice and the potential therapeutic use of adipose-derived stem cells," *Biomaterials*, vol. 33, no. 26, pp. 6105–6112, 2012.